ISBN: 978-3-95450-279-0 ISSN: 3043-0208 doi: 10.18429/JACoW-SAP2025-WEMC3

MULTIPLE-ECHO-ENABLED HARMONIC GENERATION METHOD FOR STORAGE RING LIGHT SOURCES

Weihang Liu*, Yu Zhao, Weilun Qin
Institute of High Energy Physics, Chinese Academy of Sciences, Beijing, China
Spallation Neutron Source Science Center, Dongguan, China

Abstract

Storage ring light sources (SRLS) can reuse a single electron beam to serve multiple users, offering high repetition rates and cost efficiency. However, despite the transverse emittance reaching the X-ray diffraction limit in fourth-generation SRLS, the storage ring suffers from limited longitudinal coherence. Enhancing longitudinal coherence has been shown to significantly improve spectral brightness, time resolution, and energy resolution. Laser modulation schemes for SRLS have been explored for their potential to induce strong micro-bunching, thereby enhancing spectral power and coherence. However, these methods modulate each bunch only once per revolution, limiting their application to a single beamline and underutilizing the multi-user capacity of storage rings. To enable coherent radiation delivery to multiple beamlines, we propose a multiple-echo-enabled harmonic generation scheme. This approach modulates the electron beam multiple times, generating coherent pulses at different wavelengths. By leveraging the multi-user capability of storage rings while simultaneously improving longitudinal coherence, our method enhances both spectral and temporal performance.

INTRODUCTION

Storage ring light sources have been developed from third-generation to fourth-generation, achieving approximately two orders of magnitude improvement in brightness. However, their longitudinal coherence has not been enhanced compared to third-generation sources. Improving longitudinal coherence can enhance the temporal and energy resolution capabilities of the light source, and significant advancements in these areas would provide users with a more advanced photon source. In fact, many experts believe that the next generation of storage ring light sources will possess higher longitudinal coherence.

In storage rings, the interaction between a laser and the electron beam in an undulator enables energy modulation of the beam. This energy modulation can then be converted into density modulation through longitudinal dispersion, thereby achieving micro-bunching. This micro-bunched beam can subsequently generate coherent radiation when passing through a downstream undulator [1–5]. Through this approach, the radiation performance of the light source can be substantially enhanced.

With ongoing research, similar schemes that are more suitable for storage rings and those enabling higher harmonic conversions have been progressively proposed. Figure 1 compares the implementation difficulties of several advanced seeding schemes, including echo-enabled harmonic generation (EEHG) [6–10], phase-merging enhanced harmonic generation (PEHG) [11, 12], angular dispersion-induced microbunching (ADM) [13–15], and angular modulation [12, 16], to illustrate their relative challenges. To mitigate these challenges and reduce the application complexity, the use of higher laser power is necessary. For instance, the EEHG scheme. As shown in Fig. 2, since its proposal, EEHG has been continuously explored for application in storage rings, and numerous schemes tailored for storage rings have been proposed [6–10]. By 2024, EEHG was successfully demonstrated for the first time in a storage ring [17], although the wavelength of the coherent signal obtained in the experiment did not yet meet expectations. Nevertheless, this crucial experimental validation has increased confidence in the feasibility of this approach.

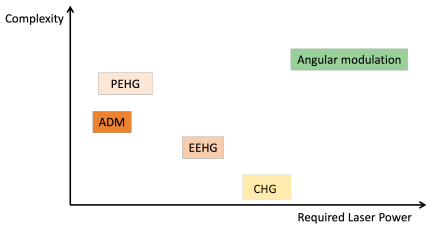

Figure 1: Implementation complexity of seeding methods in storage rings.

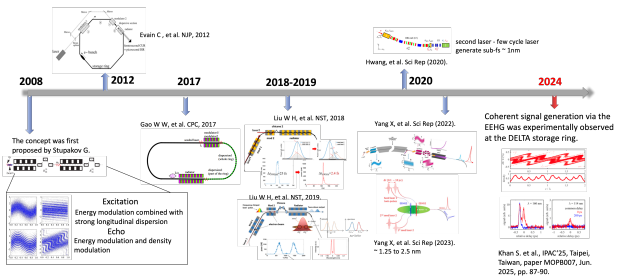

Figure 2: Development of EEHG schemes for storage rings.

However, the beam modulated by these schemes can only supply coherent radiation to a single beamline. This fundamentally differs from the conventional operation of storage rings, where a single electron bunch routinely serves multiple user beamlines with synchrotron radiation.

To enable a single electron bunch to supply coherent radiation to multiple beamlines, we propose the Multi-stage Echo-Enabled Harmonic Generation (MEEHG) method.

* liuwh@ihep.ac.cn

ISBN: 978-3-95450-279-0 ISSN: 3043-0208 doi: 10.18429/JACoW-SAP2025-WENC5

MODELING OF CSR AND ITS CANCELLATION IN DBA/CHICANE TYPE COMPRESSORS*

Fancong Zeng[1, 2], Yi Jiao[†, 1, 2], Weihang Liu[1, 3], Cheng-Ying Tsai[4]
[1]Institute of High Energy Physics, Chinese Academy of Sciences, Beijing, China
[2]University of Chinese Academy of Sciences, Beijing, China
[3]Spallation Neutron Source Science Center, Dongguan, China
[4]School of Electrical and Electronic Engineering, Huazhong University of Science and Technology, Wuhan, China

Abstract

In advanced accelerator-based light sources and colliders, bunch compressors like arc-type (DBA) and linear-type (chicane) are widely used to generate high-quality electron beams with kiloampere (kA)-level peak currents. However, a serious problem in increasing the peak current even higher is the significant degradation of beam quality caused by the Coherent Synchrotron Radiation (CSR) effect. To tackle this, we develop a new analytical model for CSR that can describe beam transport with varying bunch lengths, establish a practical framework for analyzing CSR in both DBA and chicane-type compressors, and design CSR-suppressed DBA compressors (arc-type) as well as non-symmetric C- and S-shaped chicanes (linear-type). General analytical conditions for CSR cancellation are derived for these designs. Simulations show that, with these new compressors, high beam quality can be maintained even when the peak current is increased up to 10 kA. This work provides important guidance for enhancing the performance of existing accelerator facilities, as well as for the development of next-generation accelerator-based light sources and colliders.

INTRODUCTION

The advent of accelerators and accelerator-based light sources has revolutionized advancements in science, industry, medicine, and materials research. In modern accelerators, electron bunch compressors play a pivotal role, with wide applications in linear colliders, linacs, beam driven plasma-wakefield accelerators, and significant roles in x-ray free electron lasers (FELs) [1]. Combined with the position-energy correlation provided by the rf cavity, the following dispersive element converts the energy difference into a difference in the time of flight of the particles. This effect causes the particles at the head and tail to become closer, enabling beam compression [2].

Currently, symmetric C-chicanes and DBA-based compressors are the most commonly used bunch compressors in linac-based systems and arc systems, respectively. However, due to the high peak current required for FELs, the ability to compress an electron bunch with minimal degradation of beam quality becomes challenging because of the effects of coherent synchrotron radiation (CSR). CSR is emitted for wavelengths longer than or comparable to the length of the electron bunch, and leads to detrimental tail-head inter actions in the bends [3]. The shorter and more intense the bunch is, the stronger the CSR fields produced and the more severe the CSR effects become. The emission of CSR results in projected transverse emittance growth [4]. In the past decades, various efforts have been stimulated to suppress CSR-induced emittance growth in chicane compressors, including analytical, numerical, and experimental studies [5-8]. Among them, the approach of suppressing the deleterious effects of CSR by manipulating beam optics has sparked continuing research interest.

The optical balance method was first proposed by Douglas [9] and was further developed by Courant-Snyder (C-S) formalism analysis [6]. Subsequently, the point-kick model was proposed and works well in transport systems where the bunch length remains constant or changes very little (hereafter referred to as the constant-σ_z point-kick model) [7, 8]. However, for magnetic bunch compressors, this model lacks self-consistency due to significant variations in bunch length within the bends.

To address this issue, in this study, we propose a self-consistent modified CSR point-kick model that accounts for variations in bunch length. Based on this model, we establish a practical framework for analyzing CSR in both DBA and chicane-type compressors, envisaging the potential designs for a CSR-immune DBA and chicane compressors.

Modified CSR Point-Kick Model

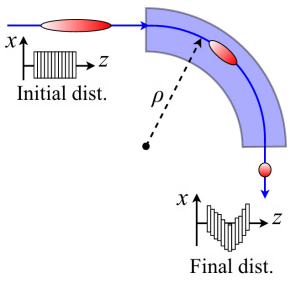

Figure 1: Schematic of the compression process after a bunch passes through a dipole, within sets of the initial and final beam distribution affected by CSR into the $x-z$ phase plane.

* Work supported by National Natural Science Foundation of China (No.12275284 and No. 12275094), the Fundamental Research Funds for the Central Universities (HUST) under Project No. 2021GCRC006, and National Key Research and Development Program of China (No.2022YFA1603402).
† jiaoyi@ihep.ac.cn

ISBN: 978-3-95450-279-0 ISSN: 3043-0208 doi: 10.18429/JACoW-SAP2025-WEXC6

BEAM EXTRACTION AND DARK CURRENT STUDY OF A C-BAND RF PHOTO GUN

Xingguang Liu*, Shimin Jiang, Shengjin Liu, Junyu Zhu, Hui Zhang, Xiao Li
Institute of High Energy Physics, Beijing, China

Abstract

We report on beam extraction and preliminary dark current studies conducted on a 3.6-cell C-band radio-frequency (RF) photocathode gun, designed for high-brightness electron beam generation. The test programme investigated the gun's performance under varying RF power, measured the resulting dark current and examined the impact of surface preparation on field emission. Particle tracking and multipacting simulations were performed to interpret the measurements. The gun achieved gradients close to 140 MV/m with photo-induced electron extraction, while significant dark current was observed at high fields. Surface analysis after the beam test revealed discharge damage on the cathode surface disk, particularly around the center area. Cleaning method comparisons were conducted, with 'snowflake' cleaning showing no detrimental effects on surface roughness. This work represents the first reported beam test for a C-band RF photocathode gun.

INTRODUCTION

Next-generation light sources and linacs require high-brightness electron beams from the beginning. Increasing the surface field of the cathode is one of the most effective ways to get smaller emittance. In Recent years, C-band RF photo guns have drawn interests among several institutes aiming to work at an extraction field of up to 180 MV/m compared to a conventional S-band gun, which typically works at 80 MV/m and higher in some test. For example, a 3.6-cell C-band RF photo gun at SARI [1] shows that it can work at 180 MV/m in high power test, while a 2.6-cell gun at INFN/PSI [2] have been tested at 160 MV/m at a very low break-down rate. Except for these standing-wave structures, travelling-wave structures have also been designed and tested recently at PSI [3]. We began to develop a 3.6-cell C-band RF gun at IHEP-Dongguan since 2021 [4]. Beam extraction has been conducted since the end of 2024. It is the first reported beam test for a C-band RF photo gun [5] and we observed the dark current is relatively very high in our gun. So we investigated this issue with simulations and surface observations after the test.

* liuxg@ihep.ac.cn

C-BAND TEST PLATFORM

The beam tests were carried out at a C-band test platform (CTP) for the development of RF photocathode and high gradient accelerating structures at IHEP-Dongguan, which is shown in Fig. 1. A brief timeline for the development of the 3.6-cell RF photo gun is:

2021.9: initial proposal
2022.1: project start
2022.4: external review
2022.12: prototype Gun-0
2023.4: prototype Gun-1 cold test
2024.7: high power test
2024.10: installation
2024.12: Beam test
2025.4: prototype Gun-2 cold test

We have an initial prototype (Gun-0) to verify the fabrication process and conducted high power test in Jul 2024 and beam test in Dec 2024 for another protoype (Gun-1).

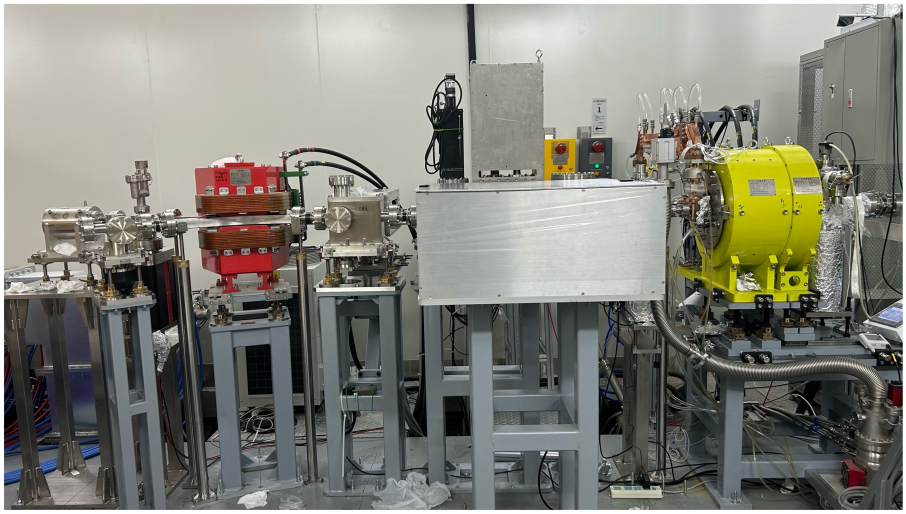

Figure 1: Test platform for the 3.6-cell RF photo gun.

ISBN: 978-3-95450-279-0 ISSN: 3043-0208 doi: 10.18429/JACoW-SAP2025-THNC3

PRELIMINARY DESIGN OF THE BEAM TRANSPORT SYSTEM FOR THE SUPER TAU-CHARM FACILITY*

Ruixuan Huang†,1, Jingyu Tang[1], Ze Yu[1], Youjin Yuan[2]
[1]University of Science and Technology of China, Hefei, China
[2]Institute of Modern Physics, Chinese Academy of Sciences, Lanzhou, China

Abstract

The injector of the Super Tau-Charm Facility (STCF) should provide high-quality electron and positron beams for the collider ring according to different injection schemes, which is one of the key systems to ensure the high brightness of STCF. This paper presents the preliminary physical design and beam dynamics optimization of the complex beam transport system, which interconnects the main accelerator components over approximately 550 meters. The design encompasses three major segments: the injection line from the positron linac to the damping ring (PL2DR), the extraction and transport line from the damping ring to the main linac (DR2ML), and the final transport lines from the main linac to the collider rings (ML2CR). Each segment addresses unique challenges, including transverse emittance preservation, Twiss parameter matching, sophisticated phase-space manipulation and tight restrictions on the geometrical conditions. Through detailed optics design and particle tracking simulations, these results demonstrate the feasibility of the transport system in maintaining the high beam quality essential for the STCF's physics program.

INTRODUCTION

The Super Tau-Charm Facility (STCF) is new-generation electron-positron collider proposed in China, aimed at in-depth research into tau-charm physics with unprecedented precision [1-3]. It is envisioned to achieve a peak luminosity of 5×10^{34} cm^{-2}s^{-1} with a center of mass energy of 2-7 GeV [4-6]. STCF will serve as a unique facility for precision measurements in the charm energy region. The injector is a sophisticated accelerator system to provide high-quality, full-energy electron and positron beams for the collider rings, serving as a key component to ensure the realization of high luminosity at STCF.

To improve the robustness of the injection process, an off-axis injection scheme is adopted, in which a schematic layout of the injector is shown as (Fig. 1) [7]. An electron beam with an intensity of 11.6 nC/bunch at 30 Hz is first generated from a thermionic gun, is then accelerated to 1.0 GeV in the first electron linac (EL1), and finally strikes a tungsten target to produce positrons. The positron beam with a bunch charge of 1.0 nC is accelerated to 1.0 GeV in the positron linac (PL) and injected into a damping ring (DR) for emittance reduction. Another electron beam with an intensity of 1.0 nC/bunch at 30 Hz is generated from a photocathode RF gun and accelerated to 1.0 GeV in the second electron linac (EL2). Both the 1.0 nC bunch charge e^-/e^+ beams are transferred to the main linac (ML) and alternately boosted to a maximum energy of 3.5 GeV. Finally, the e-/e+ beams are separated and conveyed to the e-/e+ collider rings, respectively. All the linac sections and a part of transport system are situated in the same tunnel, which will significantly reduce the construction cost.

The transport system connect the above sections and convey the electron and position beams separately from the injector to the collider rings, totally having a length of about 550 m. Optics design and beam tracking are carried out to confirm the optics matching and a sufficiently small emittance of both e-/e+ beams. The main components of the transport system are highlighted in (Fig. 1), including three parts:

(1) Injection line from PL to DR (PL2DR).
(2) Extraction and transport line from DR to ML (DR2ML).
(3) Beam transport lines from ML to CR (ML2CR).

OPTICS DEVELOPMENT

The severely short beam lifetime at STCF presents significant challenges for the injector design. For the transport system, the primary challenges include transverse emittance preservation and Twiss parameters matching. In the PL2DR, an energy-spread compression system (ECS) is carefully designed to match a very limited RF acceptance of the DR. In the DR2ML, a bunch compression system (BCS) is necessary to facilitate the transition to the ML. While in the ML2CR, tight restrictions on the geometrical conditions lead to a large curvature and a multiple horizontal-vertical bending transitions in the beam lines.

Optics of PL2DR

PL2DR is the injection line to the DR, whose length is about 90 m. It consists of a horizontal bending arc with eight 15-degree dipoles, a chicane-based ECS with four 30-degree dipoles and one 1.6-meter accelerating structure, as well as a matching unit with one 10-degree dipole. Standard FODO cells are adopted to focus the beam and realize optics matching throughout the line. As shown in (Fig. 2), the β functions at the exit of injection septum in the DR is adjusted to $\beta_{x/y}$ =9.5/4.1 m, and the dispersion is suppressed to zero, just as the DR required.

* Work is supported by the National Key R&D Program of China under Contract No. 2022YFA1602202, the National Natural Science Foundation of China (No.12341501 and 12175224) and the STCF key technology research and development project.
† rxhuang@ustc.edu.cn

ISBN: 978-3-95450-279-0 ISSN: 3043-0208 doi: 10.18429/JACoW-SAP2025-THP02

TRACKING SIMULATION OF LONGITUDINAL BEAM DYNAMICS IN A TRIPLE RF SYSTEM FOR ELECTRON STORAGE RINGS

Jincheng Xiao, Tianlong He*, Weimin Li†
National Synchrotron Radiation Laboratory, USTC, Hefei, China

Abstract

For diffraction-limited storage rings, the triple radio-frequency (RF) system has been proposed to achieve further bunch lengthening or to meet specific requirements for longitudinal injection. The choice of RF cavity parameters for the triple RF system has a significant influence on the longitudinal beam dynamics. Macroparticle tracking simulation is commonly used to accurately analyze this influence. In this paper, we extend the STABLE code to study the dynamics of the triple RF system assumed for the Hefei Advanced Light Facility storage ring. It is found that there are two important factors that possibly limit the bunch lengthening.

INTRODUCTION

The use of a double RF system to lengthen the bunch to mitigate intrabeam scattering (IBS) and Touschek scattering effects has been widely adopted in fourth-generation light sources [1,2]. More recently, a triple RF system has been proposed to further extend the bunch length and meet specific requirements for longitudinal injection. Theoretical analyses suggest that a triple RF system can approximately double the bunch lengthening capability of a double RF system [3]. However, potential instability issues, which could significantly hinder bunch lengthening, cannot be fully explored using analytical formulas.

To study longitudinal beam dynamics in double RF systems, tracking simulations are typically employed, as they provide more comprehensive, realistic, and reliable computational results. Various tracking methods have been developed for double RF systems [4–6], which are good references to implement tracking simulation for triple RF systems. In this work, we extend the STABLE code—a GPU-accelerated multi-particle, multi-bunch tracking method—by incorporating additional functional modules to enable the simulation of triple RF systems [6]. This extended code is then applied to study the assumed triple RF system for the Hefei Advanced Light Facility storage ring (HALF), which includes two HCs of order 3 and 5 (3HC and 5HC).

STABLE FOR THE TRIPLE RF SYSTEM

STABLE is a MATLAB code that comprehensively accounts for the effects of short-range wakefields, as well as the fundamental and higher-order modes of RF cavities on beam dynamics. It is used to simulate the longitudinal motion of bunches in a double RF system under arbitrary filling patterns. To enhance its capability for accurately simulating longitudinal beam dynamics in a triple RF system, relevant functional modules are integrated into the code. The process for running this code is shown in Fig. 1.

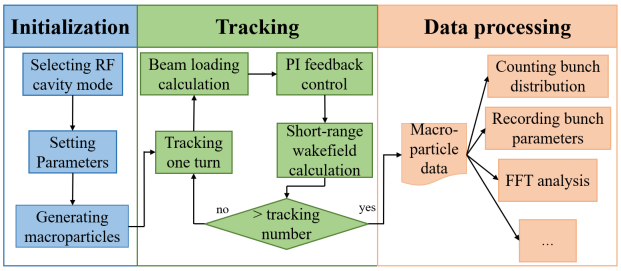

Figure 1: The flowchart of STABLE.

Related Function Modules

PI feedback module To achieve a realistic LLRF feedback for the RF cavities, a PI feedback module has been incorporated. This module first computes the error between the measured and target cavity voltages, then processes it through the PI controller to determine the corrected transmitter current, which is expressed as:

$$\Delta\tilde{I}_g(t) = \frac{\Delta\tilde{V}(t)}{R_L}K_P + \int_0^t \frac{\Delta\tilde{V}(t)}{R_L}K_I dt, \qquad (1)$$

where $\Delta\tilde{I}_g$ is the corrected generator current phasor, $\Delta\tilde{V}$ is the error cavity voltage, R_L is the loaded shunt impedance, K_P and K_I are the proportional and integral gains, respectively. Last the generator current phasor is updated with $\Delta\tilde{I}_g + \tilde{I}_{g0}$, where $\tilde{I}_{g0}$ is the initialized generator current phasor, and it is subsequently applied to the cavity voltage after a specified delay d. A detailed flowchart illustrating this process is provided in Fig. 6 of Reference [7].

Initially, this module was implemented to regulate the cavity voltage of the main cavity (MC). It was later integrated into the harmonic cavity (HC) module to enable the simulation of an active HC.

RF cavity module A dedicated higher-order HC module has been integrated into the code. To accurately simulate RF cavity under various conditions, the RF cavity module has been designed to operate in three distinct modes: ideal RF cavity, passive RF cavity, and active RF cavity.

In the ideal cavity mode, the cavity voltage remains fixed at the target voltage. In the passive RF cavity mode, the cavity voltage is determined solely by the beam loading voltage. In the active RF cavity mode, a PI feedback module is incorporated, ensuring that the total cavity voltage is the sum of the beam loading voltage and the transmitter voltage.

* htlong@ustc.edu.cn
† lwm@ustc.edu.cn

ISBN: 978-3-95450-279-0 ISSN: 3043-0208 doi: 10.18429/JACoW-SAP2025-THP03

A UNIVERSAL NUMERICAL OPTIMIZATION FRAMEWORK FOR STUDYING SEEDED FREE-ELECTRON LASER SCHEMES

Zihan Wang, Zhenghe Bai*, Guangyao Feng†
National Synchrotron Radiation Laboratory, USTC, Hefei, China

Abstract

Seeded free-electron lasers (FELs) have become indispensable tools across numerous scientific fields, owing to their high coherence and stability. To facilitate the discovery and optimization of such FELs, we propose a general-purpose framework utilizing intelligent optimization algorithms for identifying high-performance seeded FELs. In this paper, we demonstrate that our framework can automatically reproduce established seeded FELs, eliminating the need for prior physical analysis. Furthermore, this framework has the potential to discover novel schemes through the systematic incorporation of additional physical elements.

INTRODUCTION

Free-electron lasers (FELs) represent a transformative light source capable of generating high-brightness, megawatt-level pulsed beams with femtosecond-scale duration and exceptional spatial-temporal coherence [1]. A leading approach to generating short-wavelength radiation in the ultraviolet and X-ray regions is self-amplified spontaneous emission (SASE) FELs. However, SASE radiation exhibits low temporal coherence and pronounced shot-to-shot fluctuations, as the amplification process initiates from stochastic shot noise inherent in the electron beam [2].

To overcome these limitations, seeded FELs have been developed as a promising alternative. A seeded FEL operates by imprinting a periodic density modulation onto a relativistic electron beam using external coherent seed lasers and optical components. This pre-bunched beam then traverses an undulator magnet. Within the high-gain FEL regime, the induced micro-bunching is amplified through coherent emission and energy extraction, generating intense, fully coherent radiation at the seed wavelength or its harmonics. Achieving micro-bunching is the most important aspect of seeded FELs. High-gain harmonic generation (HGHG) [3] first initiates energy modulation with an external seed laser, and then converts this modulation into density modulation using a dedicated chicane. While HGHG can generate the high-order harmonic components of the seed laser frequency, its conversion efficiency decreases markedly with increasing harmonic number. Building on HGHG, echo-enabled harmonic generation (EEHG) [4] has been developed, which employs two seed lasers and two chicanes to generate a much higher harmonic density modulation in the beam from a relatively small initial energy modulation.

Different seeded FELs produce distinct micro-bunching patterns due to their unique phase space manipulation mechanisms. In this paper, we propose a general-purpose numerical framework utilizing intelligent optimization algorithms (IOA) for identifying high-performance seeded FELs. We will introduce the main components of this framework and their respective functions. Subsequently, we will illustrate its workflow and demonstrate its effectiveness with an example.

PROPOSED FRAMEWORK

The schematic layout of the optimization framework is shown in Fig. 1. It comprises five key components: (i) element definition layer, (ii) initial beam state, (iii) "black box" layer, (iv) final beam state, and (v) objective layer. The element definition layer specifies all seed lasers and optical elements available for the optimization process, with their parameters treated as variables within this framework. The initial beam state defines critical parameters of the initial beam configuration, including beam energy, relative energy spread, and phase space distribution. The "black box" layer conducts intelligent optimization by randomly selecting elements from the element definition layer along with their corresponding parameters. The final beam state characterizes the information of beam at the entrance of the radiator, which are directly determined by the initial beam state and the "black box" layer. The objective layer represents the key performance indicators for the required seeded FELs and serves as the objective functions for IOA.

First, all available seed lasers, optical elements, and critical parameters of the initial beam configuration are defined in the element definition layer and the initial beam state. These initial conditions are then passed to the "black box" layer for application of IOA. Within this layer, potential schemes are simulated. For each scheme, the resulting beam information is the final beam state at the radiator entrance. Here, by analyzing the information under the given objective functions, the potential schemes are sorted into distinct non-dominated layers. This ranking result is then utilized in the subsequent intelligent optimization cycle. Through multiple iterations of this process, seeded FEL schemes capable of achieving high performance for the specified objectives are identified.

EXAMPLE

We demonstrate our framework with an example, identifying high-performance seeded FELs that use only seed lasers for energy modulation and chicanes for density modulation. For simplicity and generality, we neglect the process in the last radiator. Considering the synchronization challenges inherent in multi-laser systems and the complexity of configuration, we configure the element definition layer with

* baizhe@ustc.edu.cn
† fenggy@ustc.edu.cn

ISBN: 978-3-95450-279-0 ISSN: 3043-0208 doi: 10.18429/JACoW-SAP2025-THP04

MINIMIZING THE FLUCTUATION OF STORAGE RING RESONANCE DRIVING TERMS USING THE STEP-BY-STEP CHROMATICITY COMPENSATION METHOD

Wanbin Li*, Yuejing Huang, Zihan Wang, Bingfeng Wei†, Penghui Yang, Zhenghe Bai‡
NSRL, University of Science and Technology of China, Hefei, China

Abstract

Our recent studies showed that reducing the fluctuation of resonance driving terms (RDTs) can enlarge the dynamic aperture (DA) of a storage ring very effectively. In this paper, we use the step-by-step chromaticity compensation method to minimize RDT fluctuations for DA optimization. For the minimization of third-order RDT fluctuations, this method yields the same optimization result as the differential evolution (DE) algorithm. Crucially, however, this method exhibits much faster convergence than the DE algorithm.

INTRODUCTION

Achieving a large dynamic aperture (DA) is a critical objective in the lattice design of a low-emittance storage ring. The numerical approach based on particle tracking is highly powerful for DA optimization but comes at the expense of high computational cost. The analytical approach based on the minimization of resonance driving terms (RDTs) was recently further developed; reducing the variation or fluctuation of RDTs along the longitudinal position is significantly more effective in increasing DA than reducing the commonly-used one-turn RDTs [1, 2]. Therefore, minimizing RDT fluctuations enables highly efficient DA optimization with substantially reduced computational cost. Instead of using evolutionary algorithms, this paper employs the step-by-step chromaticity compensation (SCC) method [3] to minimize RDT fluctuations.

THE SCC METHOD REVISITED AND MODIFICATION

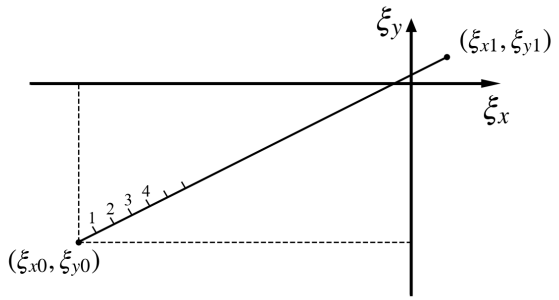

Figure 1: Schematic of the step-by-step chromaticity compensation method.

In the SCC method [3], shown in Fig. 1, the horizontal and vertical chromaticities are corrected by taking N small steps from the natural chromaticity point (ξ_{x0}, ξ_{y0}) to the desired chromaticity point (ξ_{x1}, ξ_{y1}). At each step, one pair of focusing and defocusing sextupoles (SF_i, SD_j), which provides the greatest increase in the DA area, is selected from all possible sextupole pairs to compensate for a fraction of chromaticities. The largest final DA is achieved at a reasonably large number of steps N. If N is too large, the individual contribution of each sextupole pair to the DA area becomes indistinguishable, making it hard to identify the best pair for chromaticity correction at each step. Consequently, this causes the effectiveness of the SCC method to break down.

Our recent studies found a very strong correlation between reducing RDT fluctuations and enlarging DA. Based on this correlation, the fluctuation of RDTs is used in this paper as the evaluation function to select the best sextupole pair at each step. Compared with the DA area, this evaluation function can distinguish the effects of different sextupole pairs, regardless of the number of steps N. Moreover, it significantly reduces the computational cost.

MINIMIZING RDT FLUCTUATIONS USING THE SCC METHOD

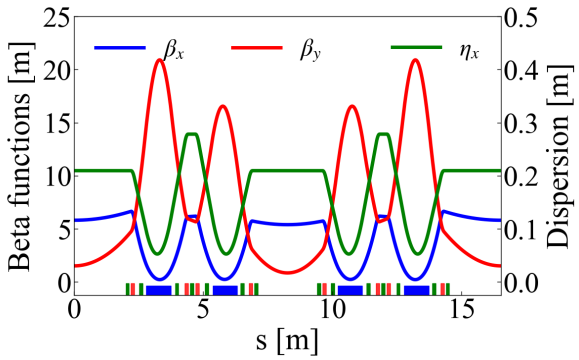

Figure 2: Linear optical functions and magnet layout of one lattice period of the HLS-III storage ring.

The HLS-III storage ring lattice [4] was used to apply and validate the SCC method. The optical functions and magnet layout of the lattice are presented in Fig. 2. The lattice has seven families of sextupoles used for chromaticity correction and nonlinear dynamics optimization. To facilitate a comparison between the SCC method with RDT fluctuations

* wanbin_li@mail.ustc.edu.cn
† weibf@ustc.edu.cn
‡ baizhe@ustc.edu.cn

ISBN: 978-3-95450-279-0 ISSN: 3043-0208 doi: 10.18429/JACoW-SAP2025-THP05

GPU-ACCELERATED SIMULATION OF LONGITUDINAL SINGLE-BUNCH INSTABILITY IN ELECTRON STORAGE RINGS

Tianlong He*, Weiwei Li, Weimin Li, Zhenghe Bai
National Synchrotron Radiation Laboratory, USTC, Hefei, China

Abstract

Longitudinal single-bunch instability driven by high-frequency impedance is a major challenge for achieving optimal performance in fourth-generation synchrotron light sources and future electron-positron colliders. Accurate simulations of this instability are critical, yet computationally intensive, often requiring millions of macro-particles and fine slicing to resolve bunch density distributions. To address this, we have developed a GPU-accelerated tracking code that enables efficient simulations of longitudinal single-bunch instability. Our solution is specifically designed to run on a desktop computer equipped with a high-performance GPU, providing an accessible and cost-effective alternative to computing clusters.

INTRODUCTION

For storage-ring light sources and electron-positron colliders, the longitudinal high-frequency dominant impedance, e.g., coherent synchrotron radiation (CSR) impedance and NEG-coating resistive wall (RW) impedance, can lead to a relatively low microwave instability (MWI) threshold current, which becomes a key factor limiting the machine performance. As a consequence, accurately computing the MWI threshold is essential for optimizing the design of a machine. Currently, there are two main types of methods that can accurately predict the MWI threshold. One is based on the Vlasov-Fokker-Planck solver, typically like the code developed by Warnock and Ellison [1], and the GPU-accelerated code of Inovesa [2]. The other is based on the macro-particle tracking, such as ELEGANT [3], its parallel version PELEGANT [4], MBTRACK [5], and its Python version MBTRACK2 [6]. This paper focuses on the tracking method. To improve the accuracy of tracking simulation, it is commonly necessary to have a sufficient number of particles and slices to accurately count the bunch density distribution and reduce numerical noise. However, this requirement undoubtedly and significantly increases the computational load, making the tracking simulation very time-consuming. To address this issue, we have developed a GPU-accelerated tracking code to significantly improve the computational efficiency of tracking simulation for MWI. We expect that this tracking code will become a useful tool for the accelerator community.

SINGLE BUNCH TRACKING WITH THE STABLE CODE

The STABLE code [7] is developed specifically for multi-bunch, multi-particle tracking simualtion for longitudinal beam dynamics. It is implemented in a MATLAB environment with the use of state-of-the-art GPU acceleration techniques, which significantly improve the tracking efficiency.

From Multi-Bunch to Single Bunch

For the original version of STABLE, the macro-particle's coordinates are stored in a 2D matrix, where each column corresponds to one bunch. In order to accurately simulate the single-bunch dynamics, which usually requires millions or even tens of millions of macro-particles, we need only modify the STABLE code by dividing the macro-particles of a single bunch into multiple parts and storing them in each column of the 2D matrix. We can separately count the bin distribution of each column and then summarize them to obtain the total bunch distribution. In addition, a fixed bin width is set by default instead of the number of bins. Therefore, the bin number will increase as the bunch lengthens. The remaining operations, such as convolution of the bunch distribution and the short-range wake (or short-bunch wake potential), and interpolation to obtain the short-range wake kick of each macro-particle, can be kept the same as those in the original version of STABLE.

Operations for Longitudinal Tracking

The longitudinal tracking in STABLE is executed to update the coordinates of macro-particles turn by turn. For convenience, the normalized quantities $q = \tau/\sigma_{\tau 0}$ and $p = \delta/\sigma_{\delta 0}$ are used. Here, τ and δ are the arrival time and relative energy deviation with respect to the reference particle, respectively. $\sigma_{\tau 0}$ and $\sigma_{\delta 0}$ are the initially given rms values of bunch length and energy spread used for normalization, which do not necessarily have to be equal to the natural rms values determined by the equilibrium between radiation damping and quantum excitation. The quantity q is updated simply with the following equation:

$$q_{i+1} = q_i + \frac{\alpha_c T_0 \sigma_{\delta_0}}{\sigma_{\tau_0}} p_i, \quad (1)$$

where α_c is the momentum compaction factor, T_0 is the revolution time, and the subscript "i" denotes the turn number. The change of p should take into account the kick factors from RF voltage, short-range wakefield, radiation damping and quantum excitation, which can be simply expressed as:

$$\Delta p = p_{i+1} - p_i = p_{RF} + p_{wake} + p_{rad.+quan.}. \quad (2)$$

* htlong@ustc.edu.cn

ISBN: 978-3-95450-279-0 ISSN: 3043-0208 doi: 10.18429/JACoW-SAP2025-THP06

PRELIMINARY SCHEME FOR ELECTRON COOLING USING LONGITUDINAL HOLLOW ELECTRON BEAM*

X. D. Yang†, He Zhao, Institute of Modern Physics, CAS, Lanzhou, China

Abstract

The intra-beam scattering in high charge state intense heavy ion beams is a problem worth considering. By controlling the longitudinal distribution of the ion beam, it may be possible to alleviate the ion beam loss and improve the lifetime of the ion beam caused by intra-beam scattering. Unlike the traditional cooling process of direct current electron beams or longitudinal uniform distribution electron bunch beams, a longitudinal hollow electron beam is used to cool heavy ion beams. Ions at the edge of the ion beam will receive stronger cooling, while ions at the center of the ion beam will receive weaker cooling, avoiding overcooling at the center of the ion beam. This paper discusses the generation, measurement, and related issues of longitudinal hollow electron beams. Corresponding solutions and suggestions have been proposed for the problems and challenges that may be encountered in the research. The cooling process of longitudinal hollow electron beams will be simulated and experimentally studied in the future, with the hope of obtaining beneficial effects.

INTRODUCTION

Intra-beam scattering is one of the main reasons of reduction of the beam intensity and shortening of stored lifetime in the collider, light source and storage ring, especially in the case of the high energy high intensity heavy ion beam with high charge state. The intra-beam scattering presents dissimilar influence in the different facilities. It can be counteracted partially by the synchrotron radiation damping in the lepton machine. It also can be suppressed by the wiggler. But there is no similar damping in the hadron machine.

The intensity and quality of ion beam in an accelerator are the most important parameters, and they are often asked to increase and improve according to the requirements of various physics experiments. High intensity beam of heavy ion with high charge state and short bunch length was expected to store in a storage ring with long lifetime and less loss.

Intra-beam scattering has become a bottleneck for maintaining the optimal performance of the accelerator. In this case, intra-beam scattering becomes the primary cause of emittance growth in the six-dimensional phase space. Particles with large amplitudes will escape the bucket and be lost in the ring. As a result, the lifetime of the ion beam in the storage ring decreases.

In order to increase the lifetime of ion beam and decrease the loss, the behavior of intra-beam scattering in the high intensity heavy ion storage ring with short bunch should be investigated completely and systemically. Electron cooling was chosen to suppress the effect of intra-beam scattering, another unexpected effect happened during the cooling.

From the perspective of beam dynamics, and based on understanding the mechanism of intra-beam scattering in high-density beams in heavy ion storage rings, more effective methods to suppress intra-beam scattering should be explored and attempted.

Under electron cooling, the distribution of ion beams quickly deviates from the initial Gaussian type, forming a denser core and a longer tail. The ions standing in the tail of the beam will be lost soon due to large amplitude [1].

A new idea was introduced in this paper. A novel solution was proposed. This novel method will be attempted to suppress intra-beam scattering. The feasibility and validity of this method was verified in this study. This idea will focus on the investigation on the suppression of intra-beam scattering in the high intensity heavy ion beam in the storage ring with the help of longitudinal hollow electron beam.

The traditional DC electron beam in the electron cooler was modulated into an electron bunch with different longitudinal distributions. The stronger cooling was expected in the tail of the ion beam and the weaker cooling was performed in the tail of the ion beam. The particle on the outside will experience stronger cooling and will be driven back into the center of the ion beam. The ion loss will be decreased and the lifetime will be increased. The intensity of the ion beam in the storage ring will be maintained for a longer period. Two functions will be combined into one electron cooler. The shorter the pulse, the higher intensity and lower emittance heavy ion beam was expected in the cooler storage ring. In the future, the results of this project will be constructive to the upgrade and improvement of existing machines and also be helpful to the design and operation of future storage and high-energy electron coolers.

MOTIVATION

From the previous experimental results [2] indicated that the partially transverse hollow electron beam has an advantage in beam accumulation. The optimal ratio Ugrid/Uanode is near 0.2 in the electron gun of electron cooling device. In this case, the centre density is 2 times less than the edge density in the electron beam.

The transverse hollow electron beam is beneficial for accumulating ion beams with higher current intensity.

The electron cooling will be expected to serve as a knob to control the longitudinal distribution of the ion beam in the storage ring.

The longitudinal hollow electron beam is expected to obtain benefits in the following aspects.

- Suppress intra-beam scattering.
- Control the longitudinal distribution of the ion beam.

* Work supported by NSFC No. 12275325, 12275323, 12205346.

† yangxd@impcas.ac.cn.

ISBN: 978-3-95450-279-0 ISSN: 3043-0208 doi: 10.18429/JACoW-SAP2025-THP07

LONGITUDINAL COLLECTIVE DYNAMICS IN LASER MODULATORS OF A STEADY-STATE MICROBUNCHING STORAGE RING BASED ON THE MACROPARTICLE MODEL

Cheng-Ying Tsai*, School of Electrical and Electronic Engineering,
Huazhong University of Science and Technology, Wuhan, China

Abstract

The mechanism of the steady-state microbunching (SSMB) storage ring is being actively investigated. In the conceptual design, a laser modulator used to modulate the electron beam include the co-propagating laser beam, undulator magnets and potential cavity mirrors, forming a laser modulator cavity. In this work the longitudinal single-bunch and multi-bunch collective dynamics are studied that may arise due to coherent undulator radiation, based on the macroparticle model. For multi-bunch multi-turn case, the dispersion equation is derived, and a detuning parameter is introduced to characterize the frequency deviation between the external laser and the resonant undulator radiation, and solve for the instability growth rates of different multibunch modes. When the detuning approaches a specific multi-bunch mode divided by the number of total microbunches, this instability mechanism tends to amplify that mode. Furthermore, possible mitigation effect of the potential well on the instability is discussed. This work may shed light on the underlying physical mechanisms of longitudinal collective beam dynamics in the laser cavity modulators of an SSMB storage ring.

INTRODUCTION

The mechanism of the steady-state microbunching (SSMB) storage ring is being actively investigated in recent years [1–20]. A distinctive feature of this mechanism is replacement of the RF cavity by a laser modulator for longitudinal focusing/modulation. The laser modulator can be implemented by a co-propagating laser along a common axis with the electron beam in an undulator. To reuse the laser beam and accumulate sufficient intensity while relaxing laser requirements, we can confine the laser beam in a closed path and configure the laser modulator as an optical cavity, called a laser modulator cavity. The existing literature for studies of electron dynamics in the laser modulators mainly focuses on single-particle effects [1–12]. The collective dynamics occurred in the laser modulators, as the next step in evaluating SSMB feasibility, has only recently been in detail studied [13–20]. In this paper we outline the main progress of longitudinal collective instability studies in laser modulators of an SSMB storage ring using the macroparticle model. An alternative approach using the beam matrix can be found in Ref. [17–19].

* Email: jcytsai@hust.edu.cn. This work is supported by the Fundamental Research Funds for the Central Universities (HUST) under Project No. 2021GCRC006 and National Natural Science Foundation of China under project No. 12275094.

UNDULATOR RADIATION WAKE

The undulator radiation (UR) impedance per unit length can be derived from its radiation energy spectrum $W_{UR}(\omega)$, i.e., $\mathrm{Re}\, Z_\parallel(\omega) = \frac{\pi}{e^2}\frac{dW_{UR}}{d\omega}$. The corresponding wake function is $W_\parallel(z > 0) = \frac{2c}{\pi}\int_0^\infty \mathrm{Re}\, Z_\parallel(k)\cos kz\ dk$ with $\omega = kc$. Figure 1 shows a typical undulator wake function.

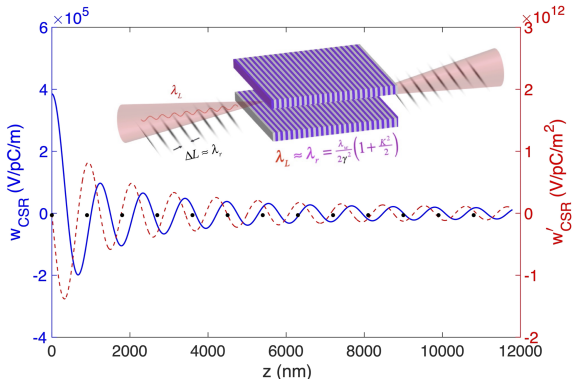

Figure 1: Undulator radiation wake function per unit length (blue solid line) and its slope (red dashed line).

SINGLE-PASS MULTI-BUNCH CASE [13]

When a microbunch train traverses the modulator undulator, every individual microbunches emit undulator radiation. On each undulator period, the wiggling motion of electron microbunches make the radiation wake advance over one resonant wavelength λ_r, affecting the leading microbunches. Denoting the index of the most trailing microbunch be 0 and that of the most leading microbunch be (N_b-1), we have the macroparticle equation of motion for the n-th microbunch

$$\frac{d^2 z_n}{ds^2} + k_{s0}^2 z_n = \frac{4\pi\epsilon_0 r_e N\eta}{\gamma}\times \sum_{j=0}^{N_b-1} W_\parallel\left[z_n - z_j + (n-j)\Delta L\right]\Theta\left(s - \lambda_w\sum_{k=j}^{n-1} N_{k+1}\right), \quad (1)$$

with $\Delta L \approx \lambda_L$, N_b the number of microbunches, k_{s0} the modulation strength characterizing the longitudinal oscillation wavenumber, $\eta = -\frac{1+\frac{K^2}{2}}{\gamma^2}$, Θ the Heaviside unit step function, and N_{k+1} the distance between the $(k+1)$-th and k-th microbunches in terms of the resonant wavelength. The set of total of n coupled differential equations can in general

ISBN: 978-3-95450-279-0 ISSN: 3043-0208 doi: 10.18429/JACoW-SAP2025-THP08

COHERENT kW THz RADIATION FROM AN SSMB STORAGE RING VIA SELF-SUSTAINED LASER MODULATION*

Cheng-Ying Tsai†, School of Electrical and Electronic Engineering,
Huazhong University of Science and Technology, Wuhan, China

Abstract

Due to the unique role of terahertz (THz) radiation in the electromagnetic spectrum, it possesses significant scientific value and potential applications in fundamental science, biomedical research, spectroscopy, and etc. This paper proposes a novel mechanism for generating continuous kilowatt-level coherent terahertz radiation in steady-state microbunching storage rings, based on self-sustaining laser modulation processes. The analysis employs the transfer matrix method from accelerator physics, considering the dynamical evolution of electron beams during multiple passes through the laser modulator, as well as radiation damping and quantum excitation effects in the storage ring. Numerical tracking results demonstrate the feasibility of this mechanism. In a demonstrative case, we show that 1 kW continuous coherent radiation can be achieved at 5 THz frequency, corresponding to electric field strengths on the order of MV/m. Since this scheme is based on free electrons, its radiation output characteristics can be tuned over a broad frequency range of 1–10 THz, offering extremely high application value in scientific research.

INTRODUCTION

Terahertz (THz) radiation holds significant scientific value and broad potential for applications across both fundamental and applied sciences. In the most demanded frequency range of 1–10 THz, existing electronic and opto-electronic systems struggle to generate high-average-power, narrowband, tunable terahertz radiation, leading to the so-called "THz gap" [1]. Currently, numerous methods exist for generating THz radiation. In this paper we propose a novel mechanism capable of generating continuous, high-average-power coherent THz radiation. As illustrated in Fig. 1, based on the steady-state microbunching (SSMB) mechanism [2, 3], this electron storage ring primarily comprises a laser modulator (LM) with laser wavelength λ_L that modulates the traversing electron beam to produce a microbunch train with bunch spacing $\approx \lambda_L$, and a radiator downstream (with target radiation wavelength λ_{THz}), where the electron beam emits the desired coherent radiation. The microbunches in the storage ring receive energy modulation from the two modulator undulators with slightly different undulator parameters. Then the microbunches with frequency-beating component will emit coherent radiation at the beating frequency in the downstream radiator. This innovative storage ring differs from conventional RF-based ones, as the electron bunch length is now determined by the phase space bucket formed by the LM, with a bucket width approximately equal to the laser modulation wavelength — at least five orders of magnitude shorter than the RF wavelength of conventional microwave cavities. To provide stable and effective energy modulation in the LM, an optical enhancement cavity (OEC) is designed to store sufficient laser power while external laser injection is typically required to compensate for cavity losses. This novel scheme significantly reduces the dependence on the external modulation laser by directly utilizing the resonant undulator radiation generated by the traversing electron beam in the LM. The proposed scheme requires the external laser modulation only very briefly during the initial stage to form a microbunch train, eliminating the need for long-term stable maintenance of external laser injection. The analysis employs transfer matrices incorporating the dynamics as the electron beam traverses the LM in successive passes, along with radiation damping and quantum excitation in the storage ring. In the demonstrated example, continuous 1 kW of coherent radiation at 5 THz can be generated.

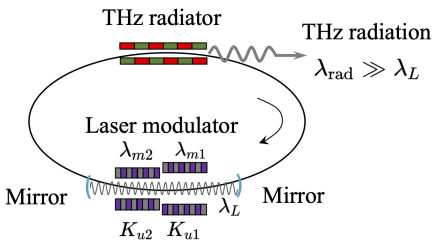

Figure 1: Schematic layout of the self-sustained infrared laser modulator (LM) based on an SSMB storage ring.

THEORETICAL MODEL

Here we summarize the basic ingredients of the theoretical model. Due to page limit, we refer the interested readers to Refs. [4–7] for more details.

- The transfer matrix of a laser modulator (LM) is described as a thick longitudinal quadrupole, in which the modulation or chirp strength $h = k_L \frac{\Delta \mathscr{E}}{\gamma mc^2}$ is evaluated from Lorentz equation for the energy exchange $\Delta \mathscr{E} = \int (d\mathscr{E}/ds) ds$ in the two modulator undulators.
- The turn-by-turn variation of modulation power in the LM is expressed as the sum of accumulated external injection laser power $P_{L,n}^{\mathrm{ext}}$ and the resonant undulator radiation power, i.e., $P_{L,n} = P_{L,n}^{\mathrm{ext}} + \delta P^{(n)}$, where the latter is evaluated according to Ref. [8].

* This work is supported by the Fundamental Research Funds for the Central Universities (HUST) under Project No. 2021GCRC006 and National Natural Science Foundation of China under project No. 12275094.

† jcytsai@hust.edu.cn

ISBN: 978-3-95450-279-0 ISSN: 3043-0208 doi: 10.18429/JACoW-SAP2025-THP09

QUASI-LINEAR THEORY OF SINGLE-PASS MICROBUNCHING INSTABILITY

Cheng-Ying Tsai*, School of Electrical and Electronic Engineering,
Huazhong University of Science and Technology, Wuhan, China

Abstract

The existing theoretical treatment of single-pass microbunching instability (MBI) typically assumes a coasting beam and adopts a linear framework, within which the microbunching gain may grow without bound. While the inclusion of intrabeam scattering (IBS) introduces damping effects that may suppress excessive gain, these models remain fundamentally linear and do not capture saturation behavior. In this work, we develop a quasi-linear theory of MBI based on the Vlasov equation, incorporating the evolution of beam energy spread induced by the instability itself. The quasi-linear formulation yields a set of coupled equations describing the evolution of the bunching factor and energy spread, still under the coasting beam approximation where different modulation wavelengths evolve independently. This approach provides a more realistic description of the nonlinear evolution of MBI and offers insight into its natural saturation mechanism.

INTRODUCTION

Microbunching instability (MBI) in a single-pass high-brightness electron beam transport has been an active research topic in the past two decades (see, for example, Refs. [1–13]). The existing theoretical treatment of single-pass MBI typically assumes a coasting beam and adopts a linear framework, within which the microbunching gain may grow without bound, i.e., there is no saturation mechanism. MBI with inclusion of intrabeam scattering (IBS) or incoherent synchrotron radiation (ISR) may cause the gain not grow too high, but still a linear theory [9–12]. Here in this paper we formulate a quasi-linear theory, which, although not including IBS/ISR, can lead to saturation when the intrinsic energy spread increases due to the instability mechanism itself. It is found that the quasi-linear theory gives a set of coupled equations for bunching factor and energy spread. Here we remark that our developed quasi-linear theory still assumes a coasting beam, i.e., the modulation wavelength is much shorter compared to the total electron duration. This implies that different modulation wavelengths do not couple in the governing integral equations.

QUASI-LINEAR THEORY

For simplicity, the following analysis assumes only the longitudinal 2-D phase space (z, δ). It is straightforward to extend the theoretical formulation to 4-D or 6-D including transverse dimensions. We start from the single particle equations of motion

$$\begin{aligned} \frac{dz}{ds} &= -\eta\delta = R'_{56}\delta \\ \frac{d\delta}{ds} &= \frac{k_{s0}^2}{\eta} z - \frac{4\pi\epsilon_0 r_e c N}{\gamma} \int_{-\infty}^{\infty} \frac{dk}{2\pi} Z_{\parallel}(k;s) b(k;s) e^{ikz} \end{aligned} \tag{1}$$

where η or R_{56} is the momentum compaction function, k_{s0} is the longitudinal oscillation wavenumber (under coasting beam approximation, $k_{s0} \to 0$), r_e is the classical electron radius, c is the speed of light, N is the number of electrons, γ is the beam reference energy in unit of rest-mass energy, and $k = 2\pi/\lambda = \omega/c$ is the modulation wavenumber. Here $b(k;s)$ is the bunching factor defined as the Fourier transform of the perturbed line density distribution (see later) and $Z_{\parallel}(k;s)$ is the high-frequency impedance per unit length. Note that $b^*(k) = b(-k)$ and $Z^*_{\parallel}(k) = Z_{\parallel}(-k)$.

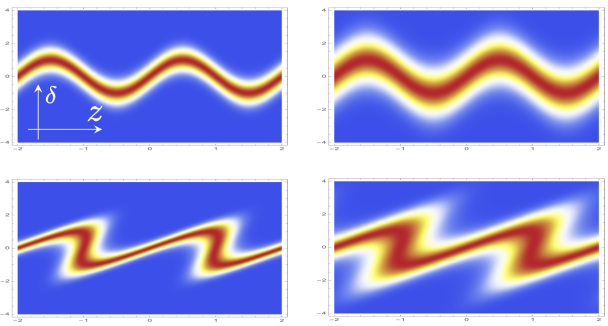

Figure 1: Illustration of intrinsic energy spread increase in the longitudinal phase space distribution.

The phase space distribution $f(z, \delta; s)$, with normalization condition $\iint f(z, \delta) = N$, follows the Vlasov equation

$$\frac{\partial f}{\partial s} + \left(\frac{dz}{ds}\right)\frac{\partial f}{\partial z} + \left(\frac{d\delta}{ds}\right)\frac{\partial f}{\partial \delta} = 0. \tag{2}$$

To simplify, we assume $f(z, \delta; s) = f_0(\delta; s) + f_1(z, \delta; s)$ with $|f_1| \ll f_0$. Now we can split the Vlasov equation into two parts: the slow equation

$$\frac{\partial f_0}{\partial s} + \left(\frac{dz}{ds}\right)\frac{\partial f_0}{\partial z} + \left(\frac{d\delta}{ds}\right)_1 \frac{\partial f_1}{\partial \delta} = 0 \tag{3}$$

and the fast equation

$$\frac{\partial f_1}{\partial s} + \left(\frac{dz}{ds}\right)\frac{\partial f_1}{\partial z} + \left(\frac{d\delta}{ds}\right)_1 \frac{\partial f_0}{\partial \delta} = 0, \tag{4}$$

where we keep the last term on LHS of Eq. (3). We note that it is this term that plays a role in the quasi-linear theory; see

* Email: jcytsai@hust.edu.cn. This work is supported by the Fundamental Research Funds for the Central Universities (HUST) under Project No. 2021GCRC006 and National Natural Science Foundation of China under project No. 12275094.

ISBN: 978-3-95450-279-0 ISSN: 3043-0208 doi: 10.18429/JACoW-SAP2025-THP10

QUICK ESTIMATE OF CSR-INDUCED MICROBUNCHING INSTABILITY IN A MULTIBEND TRANSPORT BEAMLINE

Cheng-Ying Tsai*, School of Electrical and Electronic Engineering,
Huazhong University of Science and Technology, Wuhan, China

Abstract

Microbunching instability (MBI) driven by short-range wakefields in high-brightness electron beams has been an active area of research over the past decade. While most existing studies focus on single-pass or linear accelerators — particularly few-dipole bunch compressor chicanes — MBI studies in multi-bend transport lines has relied predominantly on time-consuming numerical simulations. In this work, we present a quick estimate for evaluating MBI gain in generic multi-bend beamlines, thereby avoiding computational costs. Starting from Volterra integral equation governing the bunching factor, we first find the optimal wavelength and introduce physically motivated simplifications to derive the maximum gain. A gain spectrum is then constructed based on physical insights into MBI amplification mechanisms. The results show good agreement with detailed numerical calculations from Vlasov solver. The developed approach enables quick and reasonably accurate estimates of the MBI gain using only the lattice optics functions and the initial beam parameters, offering a practical tool for beamline design and mitigation of MBI.

INTRODUCTION

Microbunching instability (MBI) driven by short-range wakefields in high-brightness electron beams has been an active area of research over the past decade for linear accelerators (linac) [1–6] and for recirculating accelerators or energy-recovery linacs [7–15]. For a multi-bend transport line, coherent synchrotron radiation (CSR) [16–19] plays a dominant role and may lead to transverse emittance growth (see, e.g., Refs [20–22]) and/or longitudinal MBI. For a brief review, see Ref. [23]. Study of MBI can be computationally intensive through particle tracking simulations because of sensitivity to the numerical noise. Existing linearized theory is formulated based on Volterra integral equation of the second kind. Only few cases have analytical solution (based on iterative method), e.g., symmetric 3-dipole C-shape chicane [2], recently extended to arbitrary non-symmetric 4-dipole chicane [6]. For multi-bend transport lattices, there is not available quick-to-use solution; this is primarily because the MBI gain depends on lattice properties. For a generic multi-bend lattice, it is not easy to give a general formula. Therefore we need to solve the integral equation; otherwise, intense time-consuming particle tracking simulations will be performed. This work is of practical importance: instead of solving the integral equation or performing particle tracking, we give a quick estimate of maximal MBI gain and, based on knowledge of the kernel behavior, construct the gain spectrum. The required inputs are beam parameters, lattice optics, including $R_{56}(s)$ and curly-H function $\mathcal{H}_x(s)$.

* Email: jcytsai@hust.edu.cn. This work is supported by the Fundamental Research Funds for the Central Universities (HUST) under Project No. 2021GCRC006 and National Natural Science Foundation of China under project No. 12275094.

THEORETICAL FORMULATION: REVIEW

Based on the linearized Vlasov analysis, the governing equation for the bunching factor $b(k;s)$ can be formulated as a linear Volterra-type integral equation of the second kind,

$$b(k;s) = b^{(0)}(k;s) + \int_0^s K(\tau,s)b(k;\tau)d\tau, \qquad (1)$$

where $k = 2\pi/\lambda$ being the modulation wavenumber, $b^{(0)}(k;s) = b^{(0)}(k;0)\{L.D.;0,s\}$, the kernel function

$$K(\tau,s) = ik(s)R_{56}(\tau\to s)\frac{4\pi}{Z_0}\frac{I_b(\tau)}{\gamma I_A}Z_\parallel(k;\tau)\{L.D.;\tau,s\}, \qquad (2)$$

with Z_0 the free-space impedance, I_b the bunch current, γ the electron energy in unit of rest-mass energy, I_A the Alfven current, and Landau-damping {L.D.} factor

$$\{L.D.;\tau,s\} = \exp\left[-\frac{k^2}{2}U^2(s,\tau)\sigma_{\delta0}^2 - \frac{k^2\epsilon_{x0}\beta_{x0}}{2}\times \left(V(s,\tau) - \frac{\alpha_{x0}}{\beta_{x0}}W(s,\tau)\right)^2 - \frac{k^2\epsilon_{x0}}{2\beta_{x0}}W^2(s,\tau)\right] \qquad (3)$$

with $U(s,\tau) = R_{56}(s) - R_{56}(\tau)$, $V(s,\tau) = R_{51}(s) - R_{51}(\tau)$, $W(s,\tau) = R_{52}(s) - R_{52}(\tau)$ and $R_{56}(\tau\to s) = R_{56}(s) - R_{56}(\tau) + R_{51}(\tau)R_{52}(s) - R_{51}(s)R_{52}(\tau)$. Here $\sigma_{\delta0}$ is the initial slice energy spread, ϵ_{x0} the initial transverse geometric emittance, and β_{x0}, α_{x0} the initial Courant-Snyder parameters. The microbunching gain is defined as

$$G_c(k;s) = \frac{b(k;s)}{b(k;0)}, \quad G(k;s) = |G_c(k;s)|. \qquad (4)$$

For high-brightness electron beam, reduction of pure-optics bunching due to Landau damping may be neglected, i.e., Eq. (1) can be approximately written as

$$G_c(k;s) \approx 1 + \int_0^s K(\tau,s)G_c(k;\tau)d\tau. \qquad (5)$$

THEORETICAL FORMULATION: SERIES EXPANSION

Now we want to solve Eq. (5) via series expansion by writing $G_c\left(k_{opt};s\right) = \sum_{m=0}^{M} d_m s^m \Lambda^m$ with $\Lambda = \frac{I_b}{\gamma I_A}$ and

ISBN: 978-3-95450-279-0 ISSN: 3043-0208 doi: 10.18429/JACoW-SAP2025-THP11

BUNCHED-BEAM THEORY OF OF MICROBUNCHING INSTABILITY

Cheng-Ying Tsai*, School of Electrical and Electronic Engineering,
Huazhong University of Science and Technology, Wuhan, China

Abstract

Conventional theory of single-pass microbunching instability (MBI) is primarily based on the coasting-beam approximation, which assumes that the modulation wavelength is much shorter than the bunch length. However, in isochronous beamlines, the characteristic modulation wavelength may sometimes become comparable to the bunch length, rendering the coasting-beam assumption invalid. In this paper we develop a bunched-beam theory of MBI, starting from the linearized Vlasov equation, aiming to quantify the impact of finite bunch length on the evolution of density modulations. Our analysis reveals that the final MBI gain, or the amplified bunching factor, exhibits a dependence on the initial modulation phase, a feature absent in the existing coasting-beam model. The proposed bunched-beam formulation may offer additional physical insights into the underlying mechanism of MBI, particularly in regimes where the finite extent of the bunch plays a non-negligible role.

INTRODUCTION

Microbunching instability (MBI) in a single-pass high-brightness electron beam transport has been an active research topic in the past two decades (see, for example, Refs. [1–13]). The existing theoretical treatment of single-pass MBI typically assumes a coasting beam, where the modulation wavelength is much smaller compared with the total bunch duration. The coasting beam approximation significantly simplifies the Vlasov analysis and the derivation of the governing equation for the bunching factor. When the total bunch length is comparable to the modulation wavelength, the existing theory is no longer valid. An intuitive way to estimate the bunched-beam MBI gain is to convolute the MBI gain with finite-bunch spectrum. However this method may be lack of theoretical foundation. In this paper we formulate this problem starting from the linearized Vlasov equation, providing a self-consistent formulation. As demonstrated below, we find that the initial modulation phase and the finite modulation amplitude will be relevant to the final MBI gain.

VLASOV FORMULATION

Considering the only longitudinal phase space $\mathbf{Z} = [z\ \delta]^T$ and assuming that the initial phase space distribution

$$f(z,\delta;0) = \bar{f}_0(z,\delta;0) + f_1(z,\delta;0), \tag{1}$$

with $|f_1| \ll \bar{f}_0$ and the normalization condition $\int_{-\infty}^{\infty}\int_{-\infty}^{\infty} f(z,\delta)dzd\delta = N$ (here N is the number of electrons). Note that the unperturbed term has z dependence, different from the conventional MBI theory which has only δ dependence. Start from the integral form of the linearized Vlasov equation

$$f(z,\delta;s) = f(z,\delta;0) - \int_0^s \frac{\partial f_0(z,\delta;\tau)}{\partial\delta}\left(\frac{d\delta}{d\tau}\right)d\tau \tag{2}$$

where

$$\begin{aligned}\frac{d\delta}{ds} &\approx -\frac{4\pi\epsilon_0 r_e}{\gamma}\int_{-\infty}^{\infty} d\zeta W_\parallel(z-\zeta;s)n(\zeta;s)\\ &= -\frac{4\pi\epsilon_0 r_e c}{\gamma}\int_{-\infty}^{\infty}\frac{dk}{2\pi}Z_\parallel(k;s)Nb(k;s)e^{ikz}\end{aligned} \tag{3}$$

with r_e the classical electron radius, c the speed of light, γ the electron beam reference energy in unit of rest-mass energy, $W_\parallel$ or $Z_\parallel$ the wake function or impedance per unit length, n the line density, $k = 2\pi/\lambda$ the modulation wavelength and $b(k;s)$ the bunching factor defined as Fourier transform of the line density function. We define the beam sigma matrix as $\Sigma = \begin{pmatrix}\sigma_z^2 & \sigma_{z\delta}\\ \sigma_{z\delta} & \sigma_\delta^2\end{pmatrix}$, in which the chirp parameter $h = \frac{\partial\delta}{\partial z} = \frac{\sigma_{z\delta}}{\sigma_z^2}$. The Gaussian phase space distribution can be described as

$$\begin{aligned}\bar{f}_0(z,\delta;0) &= \frac{N}{2\pi\sqrt{\det\Sigma}}e^{-\frac{1}{2}\mathbf{Z}^T\Sigma^{-1}\mathbf{Z}}\\ &= \frac{N}{2\pi\sqrt{\sigma_{z0}^2\sigma_{\delta0}^2 - h^2\sigma_{z0}^4}}e^{-\frac{1}{2}\frac{1}{\det\Sigma}(z^2\sigma_{\delta0}^2+\delta^2\sigma_{z0}^2-2h\sigma_{z0}^2z\delta)}\end{aligned} \tag{4}$$

Under coasting approximation, we have $\sigma_{z0}\to\infty$ with $\frac{N}{\sqrt{2\pi}\sigma_{z0}} = n_0$. In such a situation, the prefactor becomes

$$\begin{aligned}\frac{n_0}{\sqrt{2\pi}\sigma_{\delta0}}\frac{1}{\sqrt{1-h^2\frac{\sigma_{z0}^2}{\sigma_{\delta0}^2}}} &= \frac{n_0}{\sqrt{2\pi}\sigma_{\delta0}}\frac{1}{\sqrt{1-\frac{\sigma_{z\delta}^2}{\sigma_{z0}^2\sigma_{\delta0}^2}}}\\ &\to \frac{n_0}{\sqrt{2\pi}\sigma_{\delta0}}\end{aligned} \tag{5}$$

and the exponent becomes

$$\begin{aligned}&-\frac{1}{2}\frac{1}{\sigma_{\delta0}^2\sigma_{z0}^2}\left(z^2\sigma_{\delta0}^2+\delta^2\sigma_{z0}^2-2h\sigma_{z0}^2z\delta\right)\\ &= -\frac{1}{2}\left(\frac{z^2}{\sigma_{z0}^2}+\frac{\delta^2}{\sigma_{\delta0}^2}-\frac{2h}{\sigma_{\delta0}^2}z\delta\right)\\ &\to -\frac{1}{2\sigma_{\delta0}^2}\left(\delta^2-2hz\delta\right) \approx -\frac{1}{2\sigma_{\delta0}^2}(\delta-hz)^2.\end{aligned} \tag{6}$$

* Email: jcytsai@hust.edu.cn. This work is supported by the Fundamental Research Funds for the Central Universities (HUST) under Project No. 2021GCRC006 and National Natural Science Foundation of China under project No. 12275094.

ISBN: 978-3-95450-279-0 ISSN: 3043-0208 doi: 10.18429/JACoW-SAP2025-THP12

SUPPRESSION OF EMITTANCE VARIATION FOR THE HALF STORAGE RING

Xiaoyu Liu, Zhenghe Bai*, Penghui Yang, Gangwen Liu, Zhouyu Zhao, Guangyao Feng
National Synchrotron Radiation Laboratory, USTC, Hefei, China

Abstract

The Hefei Advanced Light Facility (HALF) is a diffraction-limited storage ring light source. The HALF storage ring lattice has relatively long damping times, and the adjustment of insertion device gaps can result in substantial variations in beam emittance. This paper investigates multiple methods to suppress the emittance variation of the HALF storage ring, including the usage of damping wigglers in long straight sections, wigglers in short dispersive straight sections and leaked dispersion in long straight sections.

INTRODUCTION

The Hefei Advanced Light Facility (HALF), currently under construction and scheduled to commence trial operation in 2028, is a diffraction-limited storage ring light source operating in the soft X-ray and VUV spectral range [1]. To achieve a natural emittance below 100 pm · rad, enhanced nonlinear dynamics performance and more straight sections, the HALF storage ring design adopts a modified hybrid six-bend achromat (H6BA) lattice as its baseline configuration. The lattice optics and main storage ring parameters are shown in Fig. 1 and Table 1 [2].

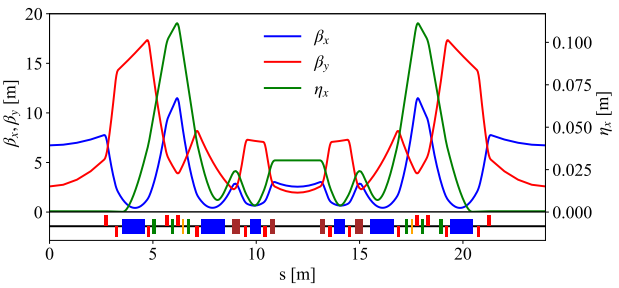

Figure 1: Linear optical functions and magnet layout of the HALF lattice. In the lower layout, bends are in blue, reverse bends in brown, quadrupoles in red, sextupoles in green and octupole in orange.

The HALF storage ring has 20 long straight sections and 20 middle straight sections, and all the experimental stations in Phase-I will employ undulators as radiation sources [3]. The Phase-I insertion devices (IDs) of HALF include 2 damping wigglers, 1 helical undulator (HU), 2 linearly polarized undulators (LPU), 6 elliptically polarized undulators (EPU) and 2 in-vacuum undulators (IVU). One short IVU will be installed in a middle straight section and the others are all in long straight sections. Table 2 shows the main parameters of the IDs at HALF.

* baizhe@ustc.edu.cn

Table 1: Main Parameters of the HALF Storage Ring

Parameter	Value
Energy	2.2 GeV
Circumference	479.86 m
Number of cells	20
Natural emittance	85.8 pm · rad
Natural energy spread	0.61×10^{-3}
Betatron tunes (H/V)	48.19 / 17.19
Natural chromaticities (H/V)	−81.6/−56.6
Momentum compaction factor	0.94×10^{-4}
Damping partitions (H/V/L)	1.36 / 1.0 / 1.64
Natural damping times (H/V/L)	28.5 / 38.8 / 23.7 ms
Energy loss per turn	181.4 keV

Table 2: Main Parameters of the HALF Insertion Devices

ID Type	λ_w [mm]	N_w	Max. K	Number
HU	115	35	8.97	1
EPU	120	33	11.26	1
EPU	63	65	5.77	1
EPU	43.5	36	2.94	2
EPU	46	90	3.29	1
EPU	41.5	99	2.67	1
IVU	20.7	182	2.10	1
IVU	20.7	52	2.10	1
LPU	38.2	108	2.83	1
LPU	38.5	108	3.36	1
Wiggler	100	42	16.00	2

In the HALF storage ring, the energy radiated in the bending magnets becomes comparable to the usually much less energy radiated in IDs. Consequently, the independent adjustment of ID gaps controlled by users can generate large random variations of emittance [4]. Several methods have been developed to suppress the emittance variation. The most common method is using compensation wigglers in long dispersion-free straight sections [5, 6], which is based on the radiation damping effect. A passive method from SPring-8-II is to leak a small amount of dispersion into each ID-equipped straight sections [7], which is based on the balance of radiation damping and quantum excitation. Other methods such as variable dispersion bump, beam momentum variation or using intra-beam scattering effect are also introduced in Ref. [4].

This paper presents a novel method based on quantum excitation effect that can suppress the emittance variation for the H6BA lattice of the HALF storage ring, and the effective-

ISBN: 978-3-95450-279-0 ISSN: 3043-0208 doi: 10.18429/JACoW-SAP2025-THP21

MODELING AND OPTIMIZATION OF TRANSVERSE TRAPPED-MODE IMPEDANCE FOR IN-VACUUM UNDULATORS OF HALF

Haiyan Yao, Xin Huang, Tianlong He*, Xiaoyu Liu, Weiwei Li, Zhenghe Bai†
National Synchrotron Radiation Laboratory, USTC, Hefei, China

Abstract

The in-vacuum undulator (IVU) exhibits exceptionally strong trapped-mode impedance due to its distinctive ridge-loaded waveguide structure and narrow magnetic gap design, which may lead to beam instability issues. This study primarily use the CST wakefield solver to investigate the trapped-mode impedance of the IVUs of the Hefei Advanced Light Facility (HALF). The trapped-mode impedance in the vertical direction is evaluated for both structures, with and without pump ports. Based on the impedance results, two mitigation strategies are proposed: ferrite damping and transition section optimization. Simulation results demonstrate that both strategies effectively reduce the impedance, with the transition section optimization strategy showing superior suppression performance.

INTRODUCTION

Modern storage-ring light sources typically employ IVUs, which consist of magnet arrays with very narrow gaps. These devices can generate photon beams with superior characteristics: higher photon energy, higher flux, and greater brightness. However, the combination of the ridged waveguide structure and the millimeter-scale magnet gaps induces strong electromagnetic interactions between the electron beam and its surroundings, creating particularly strong trapped-mode impedance in the vertical plane. This can lead to issues such as coupled-bunch instabilities. Several facilities, including Australia Light Source [1], SPEAR3 [2], BESSY II [3], PETRA-IV [4], CLS [5] and HEPS [6] have conducted relevant studies on the trapped modes of IVU.

The HALF storage ring incorporates one short and one long IVU with longitudinal lengths of approximately 1.5 meters and 4.2 meters, respectively. This paper models and simulates the short IVU under two configurations—with and without pump ports—to calculate the vertical trapped-mode impedance. Additionally, two mitigation strategies are proposed: installing ferrite damping blocks and optimizing the transition section geometry. These approaches are crucial for reducing coupling impedance and ensuring beam stability.

MODEL WITHOUT PUMP PORTS

To reduce the computational load, this study appropriately simplified the IVU model by omitting components such as cooling water pipes during the modeling process. The y–z cross-section of the simplified CST model is illustrated in Fig. 1.

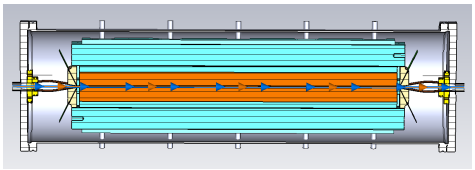

Figure 1: Model without pump ports.

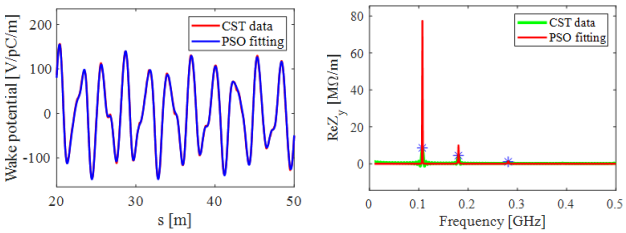

Figure 2: Results of wake potential (left) and impedance (right).

Table 1: Characteristic Parameters of the Primary Trapped Modes for the IVU Model Without Pump Ports

$f_W \mid f_E$ [MHz]	$R/Q_W \mid R/Q_E$ [kΩ/m]	$Q_W \mid Q_E$
107.2 | 106.6	154.8 | 154.0	500.1 | 547.9
180.4 | 180.3	56.6 | 52.4	176.2 | 322.0
281.4 | 281.9	9.2 | 8.4	149.2 | 313.4

The subscripts W and E denote the results from the wakefield solver and eigenmode solver, respectively.

The CST wakefield solver was primarily employed, with the bunch RMS length set to 50 mm and the offset to 1 mm. Due to partialy decay of the wakefield at 50 m, direct calculation would underestimate the impedance values. To obtain more accurate trapped-mode impedance data, the particle swarm optimization (PSO) algorithm was used to fit the wake potential and extract the characteristic parameters of the trapped modes. A comparison between the wake potential and impedance directly computed by CST and that obtained via PSO fitting is shown in Fig. 2. Three prominent impedance peaks are observed, with the strongest near 100 MHz exceeding 75 MΩ/m.

To validate the wakefield solver results, we also evaluated the impedance values of the aforementioned three modes using the CST eigenmode solver. As the simulation of the IVU model with realistic material settings required a prohibitively large mesh count and excessively long computation time, eigenmode simulations were conducted using a vacuum model (background material conductivity: 1.35×10^6 S/m). Table 1 presents the results obtained from both solvers. It can be observed that the frequencies and R/Q values of the three modes show good agreement, while certain discrepancies

* htlong@ustc.edu.cn
† baizhe@ustc.edu.cn

ISBN: 978-3-95450-279-0 ISSN: 3043-0208 doi: 10.18429/JACoW-SAP2025-THP22

EXPONENTIAL SUM FITTING OF THE LONG-RANGE TRANSVERSE RESISTIVE-WALL WAKEFIELD

Xin Huang, Haiyan Yao, Tianlong He*, Weiwei Li, Xiaoyu Liu, Zhenghe Bai, Hongliang Xu†
National Synchrotron Radiation Laboratory, USTC, Hefei, China

Abstract

In high-intensity storage rings, long-range transverse resistive-wall (RW) wakefield is a dominant source of coupled-bunch instability. Conventional particle tracking algorithms handling this wakefield require storing bunch-by-bunch and turn-by-turn centroid position histories, resulting in excessive memory consumption, which leads to computational inefficiency. This study proposes fitting the long-range transverse RW wakefield through a sum of exponentials. This method eliminates the need for bunch centroid histories during tracking computations while facilitating GPU-based parallel implementation, thereby significantly enhancing computational efficiency. This work demonstrates the dependence of the fitting performance on the number of exponential functions and the fitting interval.

INTRODUCTION

When a charged beam passes through a vacuum chamber with finite conductivity, it interacts with the chamber walls and excites electromagnetic fields, known as the resistive-wall (RW) wakefield. The RW wakefield can be categorized into the longitudinal and transverse wakefield. Among these, the long-range transverse wakefield can cause coupled bunch instability (CBI) [1, 2], which leads to beam quality degradation and, ultimately, to beam loss. Several codes, such as ELEGANT [3, 4] and MBTRACK2 [5], can simulate this effect. However, they require storing the bunch-by-bunch and turn-by-turn centroid histories, which consumes substantial memory and leads to low computational efficiency.

To address this issue, a wakefield approximation method known as resonator fitting can be employed. For instance, in the MUSIC code, M. Migliorati et al. successfully fitted the longitudinal RW impedance of the CERN Proton Synchrotron using 18 resonator functions [6]. However, as the long-range transverse RW wakefield decreases monotonically, resonator fitting is not effective. This study proposes a method to approximate the long-range transverse RW wakefield with a sum of exponentials.

Under the long-range approximation, the transverse RW wakefield of a single-layer, infinitely thick cylindrical chamber can be expressed as [7]:

$$W_{RW}^{\perp}(\tau) \approx C\frac{1}{\sqrt{\tau}}, \tag{1}$$

where C is a constant of $\frac{L}{\pi b^3}\sqrt{\frac{Z_0 c}{\pi\sigma}}$, L is the vacuum chamber length, b is the chamber radius, Z_0 is the free space impedance, c is the speed of light, and σ is the chamber material conductivity.

The long-range transverse RW wakefield is fitted using a sum of exponentials and is defined as follows:

$$\frac{1}{\sqrt{\tau}} \approx \sum_k A_k e^{-\alpha_k \tau}, \tag{2}$$

where A_k and α_k are the fitting coefficients, representing the weights and the decay factors, respectively.

Applying Eq. (2) in tracking simulations allows the wakefield kick calculation to avoid convolution with historical centroid positions. Similar to the resonator fitting method [8], this approach is well-suited for implementation on GPU parallel computing architectures, thus significantly improving computational efficiency for long-range RW wakefield induced instability simulations.

THEORY AND ALGORITHM

In the following section, we introduce two algorithms for calculating the fitting coefficients: one based on the Particle Swarm Optimization (PSO) and the other, an analytical algorithm.

PSO-Based Algorithm

Determining a set of coefficients $[A_1, \alpha_1, A_2, \alpha_2, \ldots]$ satisfying Eq. (2) can be translated into a single-objective, multivariable optimization problem. Here, the fitting coefficients serve as the variables, and the objective function is defined by:

$$f_{\text{obj}} = \int_a^b \left(f(\tau) - \frac{1}{\sqrt{\tau}}\right)^2 d\tau, \tag{3}$$

where $f(\tau) = \sum_{k=1}^{N} A_k e^{-\alpha_k \tau}$ and N denotes the number of exponential terms. This least-squares objective function quantifies the closeness of the fitted curve to the target. Minimizing it yields the optimal coefficients for approximating the long-range RW wakefield.

Commonly used optimization algorithms include the Genetic Algorithm (GA) [9], Simulated Annealing (SA) [10], and Particle Swarm Optimization (PSO) [11, 12]. In comparison to GA and SA, PSO offers distinct advantages, including fewer adjustable parameters, conceptual simplicity, and ease of implementation. Considering both its convergence speed and capability to locate the global optimum, we prioritize the use of PSO for the fitting procedure in this study.

PSO is a population-based stochastic optimization technique inspired by collective biological behavior. The configuration in this study comprised a population of 50 particles, where each particle represented a candidate coefficient set $[A_{1,i}, \alpha_{1,i}, A_{2,i}, \alpha_{2,i}, \ldots]$. The optimization was run

* htlong@ustc.edu.cn
† hlxu@ustc.edu.cn

ISBN: 978-3-95450-279-0 ISSN: 3043-0208 doi: 10.18429/JACoW-SAP2025-THP24

STUDY OF BUNCH LENGTHENING WITH HARMONIC CAVITIES FOR HLS-III

Wenshu Liang, Tianlong He*, Weiwei Li, Xiaoyu Liu, Zhenghe Bai†, Qing Luo‡
National Synchrotron Radiation Laboratory, USTC, Hefei, China

Abstract

NSRL recently proposed a future plan to further upgrade the HLS to an EUV diffraction-limited storage ring, named HLS-III. To improve the Touschek lifetime and suppress beam instabilities, HLS-III will employ a bunch-lengthening harmonic cavity system. Based on theoretical analysis, this work evaluates the bunch lengthening performance under five distinct double RF configurations involving different frequencies and harmonic orders, identifies the required harmonic cavity voltage to achieve the target bunch lengthening, and quantifies the corresponding improvement factor in Touschek lifetime. These findings provide valuable guidance for the selection of RF frequencies and the design of harmonic cavity parameters for HLS-III.

INTRODUCTION

The HLS-III upgrade proposal of HLS-II aims to achieve lower emittance and higher beam brightness. Key design parameters of HLS-III are summarized in Table 1, including a beam energy of 800 MeV, a circumference of approximately 66 m, and a natural emittance of 2.82 nm · rad—representing an order-of-magnitude reduction compared to HLS-II [1]. Similar to modern diffraction-limited storage ring light sources, HLS-III will employ harmonic cavities (HCs) for bunch lengthening to enhance beam quality by improving beam lifetime, suppressing emittance growth due to intra-beam scattering (IBS), and mitigating beam instabilities.

Table 1: Main Parameters of the HLS-III Storage Ring

Energy	800 MeV
Circumference	66.1308 m
Number of cells	4
Natural emittance	2.82 nm·rad
Momentum compaction factor	6.74×10^{-3}
Natural energy spread	4.99×10^{-4}
Natural damping times (x/y/z)	16.3 / 23.6 / 15.1 ms
Energy loss per turn	20 keV

This paper presents a theoretical analysis of bunch lengthening with harmonic cavities in HLS-III. By solving the Haïssinski equation for a double-RF system [2], we evaluate the bunch lengthening performance and corresponding cavity voltage requirements for several harmonic orders at two RF frequencies (204 MHz and 500 MHz). It should be noted that the two RF frequencies are considered for distinct reasons: the 204 MHz option is retained due to the availability of existing main cavities (MCs), though their higher-order modes (HOMs) remain undamped, posing a risk of coupled-bunch instabilities; the 500 MHz option represents a mature, commercially available technology with well-damped HOMs, aligning with current state-of-the-art practices.

THEORY AND METHOD

For the double-RF system, the total cavity voltage can be expressed as:

$$V_T(\tau) = V_1 \sin(\omega_{rf}\tau + \varphi_1) + kV_1 \sin(n\omega_{rf}\tau + \varphi_n), \quad (1)$$

where V_1 denotes the MC voltage amplitude, $k = V_n/V_1$ represents the voltage ratio of the HC to the MC, φ_1 and φ_n are the synchrotron phases of MC and HC, ω_{rf} is the angular radio-frequency, and n is the harmonic order of HC [3].

The value of V_1 can be determined based on the momentum acceptance requirement. For a single-RF system, the momentum acceptance is given by:

$$\delta_{\text{acc}} = \sqrt{\frac{2eV_1}{\pi h \alpha_c E_0} \times \left|\cos\varphi_s + \left(\varphi_s - \frac{\pi}{2}\right)\sin\varphi_s\right|}, \quad (2)$$

where e is the electron charge, φ_s is the synchronous phase ignoring HC, α_c denotes the momentum compaction factor, E_0 is the electron energy, and h is the harmonic number.

By setting the first and second derivatives of the total cavity voltage to zero, the well-known optimal-lengthening condition is obtained [4]:

$$\sin(\varphi_{1,fp}) = \frac{n^2}{n^2-1}\frac{U_0}{eV_1}, \quad (3)$$

$$k_{fp} = \sqrt{\frac{1}{n^2} - \frac{1}{n^2-1}\left(\frac{U_0}{eV_1}\right)^2}, \quad (4)$$

$$\tan(\varphi_{n,fp}) = -\frac{nU_0}{eV_1}\frac{1}{\sqrt{(n^2-1)^2 - \left(\frac{n^2U_0}{eV_1}\right)^2}}, \quad (5)$$

where k_{fp}, $\varphi_{1,fp}$, and $\varphi_{n,fp}$ denote the voltage ratio between HC and MC, synchronous phases for MC and HC under the optimal-lengthening condition, respectively.

The longitudinal RF potential, which determines the equilibrium density distribution, is given by [5]:

$$\Phi_{\text{RF}}(\tau) = \frac{eV_1}{2\pi h E_0 \alpha_c \sigma_\delta^2}\{\cos(\varphi_1) - \cos(\omega_{\text{rf}}\tau + \varphi_1) + \frac{k}{n}[\cos(\varphi_n) - \cos(n\omega_{\text{rf}}\tau + \varphi_n)] - \frac{U_0\omega_{\text{rf}}\tau}{eV_1}\}, \quad (6)$$

* htlong@ustc.edu.cn
† baizhe@ustc.edu.cn
‡ luoqing@ustc.edu.cn

ISBN: 978-3-95450-279-0 ISSN: 3043-0208 doi: 10.18429/JACoW-SAP2025-THP34

ANALYTICAL STUDY OF FRINGE FIELDS AND NONLINEAR TRANSPORT IN A SECTOR-BASED ENERGY ANALYSIS SYSTEM*

Y. Wang†, Y. Zeng†, D. Xiao†, H. Hu, K. Liu, T. Hu‡
Huazhong University of Science and Technology, Wuhan, China
Y. Lu, G. Feng, University of Science and Technology of China, Hefei, China

Abstract

Energy Analysis (EA) systems based on sector magnets are widely applied in accelerators. Nevertheless, for low-energy electron beams below 15 MeV, extra measurement errors introduced by fringe fields of the sector magnet cannot be neglected. Moreover, initial beams with large momentum spread will encounter system errors arising from nonlinear transport. Such fringe-field-induced aberrations and their impact on momentum spectrum are studied analytically and a compensation scheme considering high-order momentum spread terms is proposed. Further, the theoretical derivation is validated with simulations, and correction of second-order aberration errors is explored via data processing. These methods and conclusions improve the accuracy of built/operational EA systems without extra costs.

INTRODUCTION

Injectors are regarded as core components of various electron accelerator–based facilities [1, 2]. Accurate measurement of the momentum distribution for the beam injectors is vital for the necessary facility. The energy analysis method based on magnetic deflection is widely applied in various domestic and international accelerator facilities [3–5], owing to its simple structure, high resolution, and ease of implementation.

This method is implemented by combining the dispersion effect of the sector magnet with beam transport theory, through which the momentum spectrum of the electron beam is obtained by measuring the bunch size at the downstream end of the EA system [6, 7]. When a electron with initial transverse offset x_0, angular deviation x_0', and momentum deviation δ passes through a system characterized by a transfer matrix M, the horizontal displacement at the the system end can be expressed as $x_1 = m_{11}x_0 + m_{12}x_0' + m_{13}\delta$ [8], where m_{11}, m_{12} and m_{13} are the corresponding elements of M.

However, in the measurement of low-energy beams with large momentum spread, the momentum spectrum errors caused by fringe fields and nonlinear transport effects are often neglected in conventional magnetic deflection methods [9–11]. The analytical expression for the longitudinal beam transport in the sector magnets is derived through the analysis of its fringe fields and the nonlinear transport process, and the sources of momentum dispersion measurement errors and their correction methods are further explored in this study.

ANALYTICAL STUDY OF FRINGE-FIELD-INDUCED ERRORS

For convenience, the magnet is divided into three sections along the s direction: the entrance and exit fringe field regions and the bending region. Only the main magnetic field is typically considered in conventional sector-magnets analysis. Momentum spectrum errors are caused by the neglected fringe fields [12], necessitating in-depth analysis of dynamical effects [13, 14].

To focus on the effect of the fringe fields, assuming $\delta = 0$. Starting from the Hamiltonian equation, the magnetic field components of the fringe fields are substituted into the equations of motion and integrated within the fringe regions [15, 16]. Neglecting high-order terms, the expression for a electron with the initial state $(x_0, p_{x_0}, y_0, p_{y_0})$ after passing through the entrance fringe field region is obtained as follows, where x_0 and y_0 denote the position offsets in the x and y, p_{x_0} and p_{y_0} represent the angular deviations, ρ denotes the bending radius, and p_z denotes the longitudinal momentum of the electron:

$$\begin{cases} x_1 = x_0 + \dfrac{y_0^2}{2\rho p_z}, \\ p_{x_1} = p_{x_0}, \\ y_1 = y_0, \\ p_{y_1} = p_{y_0} - \dfrac{y_0 p_{x_0}}{\rho p_z}. \end{cases} \tag{1}$$

The effect of the bending region is described directly by the first-order linear transfer matrix, and the expression of the electron after traversing the bending region is thereby obtained as follows:

$$\begin{cases} x_2 = \dfrac{\cos\theta}{2\rho p_z} y_0^2 + x_0 \cos\theta + \rho p_{x_0} \sin\theta, \\ p_{x_2} = -\dfrac{\sin\theta}{2\rho^2 p_z} y_0^2 - \dfrac{\sin\theta}{\rho} x_0 + p_{x_0} \cos\theta, \\ y_2 = \left(1 - \dfrac{p_{x_0}\theta}{p_z}\right) y_0 + \rho\theta p_{y_0}, \\ p_{y_2} = -\dfrac{p_{x_0}}{\rho p_z} y_0 + p_{y_0}. \end{cases} \tag{2}$$

Then the electron motion through the exit fringe field region is integrated by the same analytical method as the entrance

* Work supported by the National Natural Science Foundation of China (No.1257051916 and No.12341501) and the National Key R & D Program of China (No.2024YFA1612200)

† Equal contribution
‡ TongningHu@hust.edu.cn

ISBN: 978-3-95450-279-0 ISSN: 3043-0208 doi: 10.18429/JACoW-SAP2025-THP37

PHYSICAL DESIGN OF MICROWAVE ELECTRON GUN OPTIMIZED FOR CARBON NANOTUBE CATHODES*

Tianhui He†
Institute of Applied Electronics, Chinese Academy of Engineering Physics, Mianyang, China

Abstract

Since the maximum electric field strength that a carbon nanotube field-emission cathode can withstand is less than 13 MV/m, the optimization scheme of shortening the length of the first cavity based on the traditional 1/2+1 cavity-type microwave electron gun fails to solve the problems of electron phase slippage and back-bombardment. Therefore, in accordance with the emission characteristics of the carbon nanotube field-emission cathode, beam dynamics optimization was conducted on different cavity structures to select a more suitable cavity structure. Subsequently, the radio frequency (RF) design of the electron gun was completed through fine parameter adjustment of the cavity structure. Finally, the engineering design of the electron gun was accomplished after considering multiple aspects such as the gun's assembly, cathode structure, microwave feed-in structure, and electron beam output structure.

INTRODUCTION

Cold cathodes, as devices that can achieve electron emission without external heating, have become a research focus in the field of vacuum electronics due to their characteristics such as fast response, compact structure, and low power consumption. With the development of materials science, their material system has expanded from traditional metal tips and diamond films to carbon nanotubes (CNTs) and two-dimensional materials. Their emission performance and stability have been continuously improved, and cold cathode electron guns have also been initially applied in fields such as small vacuum devices and pulsed power systems. However, challenges remain in the generation of high-brightness and high-stability beams, especially in the practical application in the accelerator field [1, 2].

In the accelerator field, the performance of electron sources directly restricts beam quality and system efficiency. Compared with traditional hot cathodes, cold cathodes do not require preheating, which can shorten start-up time, avoid energy waste caused by heat loss, simplify structural design and reduce operating costs. Their fast-switching characteristic also enables precise regulation of pulsed beams, providing a new path for scenarios with strict requirements on time resolution, such as free-electron lasers and medical radiotherapy [3, 4]. Therefore, the development of cold cathode microwave electron guns is crucial for the miniaturization and integration of accelerators.

CNTs, with their high aspect ratio, excellent electrical conductivity, and low work function, have a low field emission threshold and high current density, making them ideal candidate cathodes for microwave electron guns [5]. However, when applied to existing platforms, due to their low electric field strength tolerance (less than 13 MV/m), while microwave electron guns require a high electric field in the cavity for strong-field acceleration, severe electron back bombardment occurs, resulting in cathode surface damage and performance degradation [6, 7].

To address this issue, this paper optimizes the physical design of the microwave electron gun based on the characteristics of CNTs cathodes: shortening the cavity length to reduce the residence time of electrons in the cavity, and introducing a nose cone structure to optimize the microwave electric field distribution. Simulation results show that after optimization, the electron back bombardment phenomenon is significantly reduced, laying a foundation for the practical application of CNTs cathodes in microwave electron guns.

RF-GUN DESIGN

In 2023, we established a cold cathode test platform based on a single-cavity 0.38-cell RF-gun, on which the field emission characteristics of a series of carbon nanotube thin-film cathodes and diamond thin-film cathodes were tested. Based on the more representative test results among them, we designed a single-cavity RF-gun using a carbon nanotube thin-film cathode.

Field Emission Characteristics of CNTs

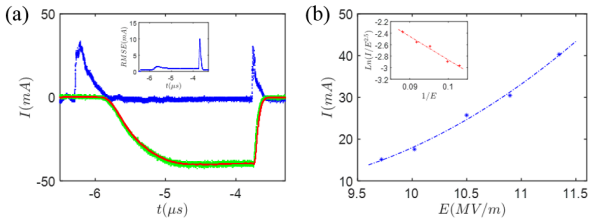

Figure 1: Test Results: (a) Field emission current waveform and reflection waveform; (b) Fitting curve of field emission characteristics.

The results of the CNTs thin-film cathode are shown in Figure 1. Among them, Figure 1(a) contains three characteristic curves: the blue curve represents the microwave reflection waveform, the green curve represents the macro-pulse current waveform, and the red curve is the smoothed curve of the macro-pulse current waveform; Figure 1(b) is the F-N fitting curve for the field emission characteristics.

The maximum field-emission current of the CNTs thin-film cathode is approximately 40 mA (with a cathode field-emission diameter of 6 mm and a current density of 0.14 A/cm²), among which the field enhancement factor is

* Work supported by Infrared terahertz free electron laser device project.
† htth111@163.com

ISBN: 978-3-95450-279-0 ISSN: 3043-0208 doi: 10.18429/JACoW-SAP2025-THP42

SPECTRAL FORM FUNCTION WITH APPLICATIONS IN BEAM PHYSICS

Xiujie Deng*, Institute for Advanced Study, Tsinghua University, Beijing, China

Abstract

To describe longitudinal fine structure like microbunching within a particle beam, a classical approach is to define a bunching factor which is the Fourier transform of the particle longitudinal density distribution. Such a 1D definition of bunching factor can be generalized to a 6D spectral form function (SFF) to describe more complicated structure in phase space. The complex SFF is another complete description of beam in spectral domain and can offer complementary and valuable insight in beam dynamics study which usually invokes the real particle density distribution. The basic property and Fokker-Planck equation of the SFF is presented, along with its solution in a general coupled linear lattice. The example applications of SFF in electron storage ring physics and laser-induced microbunching are presented.

INTRODUCTION

Microbunching enables laser-like radiation generation from charged particle beam, and is one of the main driving forces advancing accelerator light sources in the past decades. The most prominent example is free-electron laser. Usually we mainly care about the longitudinal coordinate of the particles in quantifying the degree of microbunching, since the radiation of a relativistic beam is dominantly in the forward direction. But strictly speaking the 6D particle phase space coordinates can all have an impact on coherent radiation [1]. One can even create novel 6D structures in phase space for various purposes, for example to tailor the radiation properties or to control collective beam dynamics. One example is the creation of helical microbunching for light generation with orbit angular momentum [2]. The classical 1D definition of bunching factor is clearly not sufficient in many applications. This justifies our motivation to investigate such a generalized definition of spectral form function (SFF). But we recognize the potential applications of SFF can be much broader than this original motivation.

SPECTRAL FORM FUNCTION

6D particle state vector: $\mathbf{X} \equiv \begin{pmatrix} x & x' & y & y' & z & \delta \end{pmatrix}^T$. 6D spectral vector: $\mathbf{K} \equiv \begin{pmatrix} k_x & k_{x'} & k_y & k_{y'} & k_z & k_\delta \end{pmatrix}$. Normalized charge density function: $\psi(\mathbf{X})$ satisfying $\int \psi(\mathbf{X}) d\mathbf{X} = 1, \psi(\mathbf{X}) \geq 0$. Then SFF is defined as:

$$\mathcal{F}(\mathbf{K}) \equiv \int \psi(\mathbf{X}) e^{-i\mathbf{K}\mathbf{X}} d\mathbf{X}. \tag{1}$$

$\psi(\mathbf{X})$ and $\mathcal{F}(\mathbf{K})$ forms a Fourier transform pair

$$\psi(\mathbf{X}) = \frac{1}{(2\pi)^6} \int \mathcal{F}(\mathbf{K}) e^{i\mathbf{K}\mathbf{X}} d\mathbf{K}. \tag{2}$$

* dengxiujie@mail.tsinghua.edu.cn

The linear symplectic dynamics in an accelerator is dictated by a quadratic Hamiltonian $\mathcal{H} = \frac{\mathbf{X}^T\mathbf{H}\mathbf{X}}{2}$, where $\mathbf{H} = \mathbf{H}^T$. The Hamiltonian equation in matrix form is then $\frac{d\mathbf{X}}{ds} = \mathbf{S}\mathbf{H}\mathbf{X}$, with $\mathbf{S}$ the symplectic form. The evolution of particle state vector from the initial point s_i to the final point s_f can be described by a symplectic transfer matrix according to $\mathbf{X}(s_f) = \mathbf{R}(s_f, s_i)\mathbf{X}(s_i)$, with $\mathbf{R}(s_f, s_i) = e^{\int_{s_i}^{s_f} \mathbf{S}\mathbf{H} ds}$ if $\mathbf{H}$ is s-independent from s_i to s_f. Correspondingly the transfer matrix for $\mathbf{K}$ is $\mathbf{K}(s_f) = \mathbf{K}(s_i)\mathbf{R}^{-1}(s_f, s_i)$. From continuity equation $\frac{\partial \psi}{\partial s} + \nabla_{\mathbf{X}} \cdot \left(\psi \frac{d\mathbf{X}}{ds}\right) = 0$ where $\nabla_{\mathbf{X}} \equiv \left(\frac{\partial}{\partial \mathbf{X}_1}, \cdots, \frac{\partial}{\partial \mathbf{X}_6}\right)$ and Hamiltonian equation follows the Liouville equation

$$\frac{d\psi}{ds} = \frac{\partial \psi}{\partial s} + [\psi, \mathcal{H}] = 0, \frac{d\mathcal{F}}{ds} = \frac{\partial \mathcal{F}}{\partial s} + [\mathcal{H}_{\mathbf{K}}, \mathcal{F}] = 0, \tag{3}$$

with $\mathcal{H}_{\mathbf{K}} = -\frac{\mathbf{K}\mathbf{S}\mathbf{H}\mathbf{S}\mathbf{K}^T}{2}$, from which follows $\psi(\mathbf{X}, s_f) = \psi(\mathbf{R}^{-1}(s_f, s_i)\mathbf{X}, s_i)$, $\mathcal{F}(\mathbf{K}, s_f) = \mathcal{F}(\mathbf{K}\mathbf{R}(s_f, s_i), s_i)$. We recognize the work presented in this section has been obtained before by Yampolsky [3].

FOKKER-PLANCK EQUATION

Now let us add non-symplectic process, like damping and diffusion. Here we simplify the discussion by assuming that the damping coefficients are independent of the particle state vector, for example that of the radiation damping. The equation of motion is now

$$\frac{d\mathbf{X}}{ds} = (\mathbf{S}\mathbf{H}\mathbf{X} + \mathbf{B}\mathbf{X}) + \xi(s), \tag{4}$$

with the stochastic process ξ satisfying $\int p(\xi) d\xi = 1$, $\int \xi_i p(\xi_i) d\xi_i = 0$, $\int \xi_i(s)\xi_j(s') p(\xi_i(s), \xi_j(s')) d\xi_i d\xi_j = D_{ij}\delta(s - s')$, where $p(\xi)$ is the probability distribution function of ξ. We have assumed that the noise is a Gaussian white noise. In the above equation, $\mathbf{B}$ is responsible for the deterministic damping or antidamping, and ξ for diffusion. Note that here we actually assume that the diffusion is a continuous-diffusion process, instead of a jump-diffusion process whose rigorous description requires the Kramers-Moyal expansion [4]. The quantum excitation for example is more accurately modeled by a jump-diffusion process. Denote $\mathbf{C} \equiv \mathbf{S}\mathbf{H} + \mathbf{B}$, and note that $\mathrm{Tr}(\mathbf{S}\mathbf{H}) = 0$, we can then derive the Fokker-Planck equation for $\psi(\mathbf{X})$

$$\frac{\partial \psi}{\partial s} + \nabla_{\mathbf{X}} (\psi \mathbf{C}\mathbf{X}) = \frac{1}{2} \sum_{i=1}^{6} \sum_{j=1}^{6} D_{ij} \frac{\partial^2 \psi}{\partial \mathbf{X}_i \partial \mathbf{X}_j}. \tag{5}$$

The corresponding equation in spectral domain is

$$\frac{\partial \mathcal{F}}{\partial s} - (\mathbf{K}\mathbf{C})(\nabla_{\mathbf{K}} \mathcal{F}) = -\frac{\mathbf{K}\mathbf{D}\mathbf{K}^T}{2} \mathcal{F}, \tag{6}$$

ISBN: 978-3-95450-279-0 ISSN: 3043-0208 doi: 10.18429/JACoW-SAP2025-THP44

PHYSICAL DESIGN STUDY OF THE MAIN MAGNET FOR THE CIAE 75 MeV CYCLOTRON*

JinRong Lu †, TianJian Bian, ShiZhong An, SuMin Wei, LuYu Ji
China Institute of Atomic Energy, Beijing, China

Abstract

A 75 MeV cyclotron is currently under development at the China Institute of Atomic Energy (CIAE). This cyclotron is designed to extract a beam with a rated power exceeding 60 kW for the production of medical radioisotopes, such as ^{68}Ge, ^{223}Ra, and ^{225}Ac, aiming to meet the growing domestic demand for diagnostic and therapeutic radionuclides. This paper addresses key challenges and solutions in the design and computational analysis of the main magnet. The magnet poles adopt a structural design scheme featuring integrated straight-edged sectors with a slight spiral angle at the trailing edges. The isochronous magnetic field distribution is achieved through an axial shimming method. Magnetic field optimization was performed using the numerical simulation software OPERA-3D, thereby enhancing the acceleration efficiency of the cyclotron. Furthermore, deformation simulation and mechanical structural optimization were carried out for the main magnet. Under the premise of ensuring overall performance, the deformation of the main magnet—which has a diameter of 4.4 meters and a weight of 130 tons—was controlled within acceptable engineering tolerances.

INTRODUCTION

CIAE has been a pioneer in the development of cyclotrons in China. Over decades of progress, it has successfully designed and constructed a series of high-intensity cyclotron facilities. Building upon the team's extensive experience and technical foundation in cyclotron technology, we propose the design and construction of a new high-intensity cyclotron capable of delivering an extracted beam of 75 MeV with a current of 800 μA.

This cyclotron will employ an external ion source for high-current beam injection. Through the implementation of high-efficiency injection and extraction systems, highly stable automated magnetic field mapping, and high-precision axial shimming techniques, the machine is designed to achieve low beam loss. Furthermore, an optimized compact structure significantly reduces the overall size and weight of the machine, improving both integration and engineering feasibility.

MAGNET DESIGN

The main magnet system constitutes one of the key subsystems of the cyclotron. Its physical design follows an iterative optimization process based on beam dynamics requirements, aiming to ensure that the magnetic field distribution satisfies fundamental beam dynamics conditions. The system adopts a four-fold symmetric structure. The magnet poles are designed as straight-sided sectors, which not only enhances the overall symmetry of the cyclotron but also facilitates the design and installation of critical components such as the central region.

At large radii, a specific spiral angle is introduced on the pole sides to strengthen the axial focusing capability in this region, thereby preventing the particle working orbit from crossing dangerous resonance lines. This design allows for an increase in the pole angular width by reducing the magnetic flutter, which in turn raises the average magnetic field strength and ultimately contributes to the compactness of the machine. The actual pole angle in this design is set to 53°. Furthermore, the influence of the Lorentz force-induced stripping effect on beam loss must be considered during the magnetic field design process, the peak magnetic field is limited to below 1.55 T. To avoid breakdown risks in the central region electrode structure and to provide sufficient space for an automated field mapping system, the hill gap in this design has been significantly enlarged compared to previous high-intensity cyclotrons. The hill gap ranges from 3.8 cm to 4.6 cm and features an elliptical profile to improve the pole utilization efficiency.

The total weight of the main magnet system (including shimming bars) for this high-intensity cyclotron is 130 tons, with overall dimensions of 4.3 m (length) × 4.3 m (width) × 1.56 m (height). The system specifically comprises 2 cover plates, 4 return yokes, 8 magnet poles, 8 shimming bars, and 2 central region core columns. The detailed structure is shown in Fig.1, and the dimensional parameters are listed in Table 1.

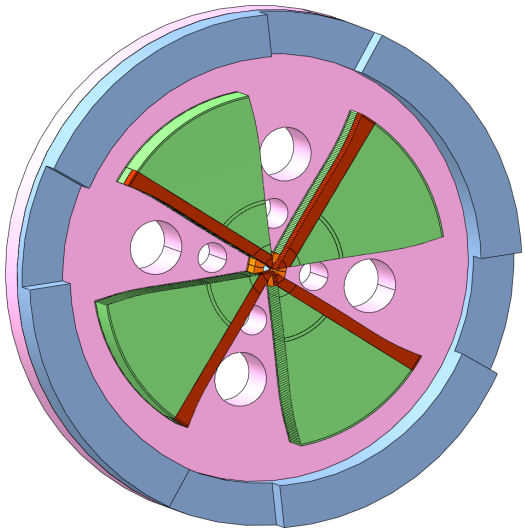

Figure 1: A top view on the 75MeV Cyclotron of CIAE.

* Work supported by the National Natural Science Foundation of China (Grant No.12105370)
† 359037465@qq.com.

ISBN: 978-3-95450-279-0 ISSN: 3043-0208 doi: 10.18429/JACoW-SAP2025-FRMC6

REAL-TIME COMPREHENSIVE ELECTRON BEAM DIAGNOSTICS THROUGH MACHINE LEARNING IN ULTRAFAST ELECTRON DIFFRACTION SYSTEM

Jiapeng Li, Cheng-Ying Tsai*, Kuanjun Fan, School of Electrical and Electronic Engineering, Huazhong University of Science and Technology, Wuhan, China

Abstract

Mega-electron-volt (MeV) ultrafast electron diffraction (UED) is a powerful technique for observing atomic-scale structural dynamics in materials. Electron beam parameters, e.g., beam size, divergence, energy spread, and bunch length, determine spatio-temporal resolution. Traditional diagnostic methods require complex instrumentation that cannot be integrated into routine workflows, particularly for high-repetition-rate facilities. We present a machine learning approach enabling comprehensive, non-invasive extraction of electron beam parameters directly from diffraction patterns. Deep neural networks trained on physics-based simulations decode signatures that beam parameters imprint on diffraction images. The method exploits distinct physical mechanisms: geometric effects from beam size, angular distortions from divergence, chromatic aberrations from energy spread, and temporal convolution from bunch length. This enables bunch length measurement without dedicated temporal diagnostics — traditionally one of the most challenging parameters to access non-invasively. The trained models can be deployed across UED facilities using standard imaging detectors, democratizing access to advanced diagnostics. This approach eliminates expensive specialized equipment and enables real-time beam monitoring and optimization, enhancing experimental throughput and data quality for ultrafast materials characterization.

INTRODUCTION

MeV ultrafast electron diffraction (UED) [1–3] employs the pump-probe technique to observe atomic-scale dynamic processes with femtosecond temporal resolution. Experimental success will depend highly on electron beam quality, including beam size, divergence, energy spread, and bunch length. Existing machine learning methods only predict partial beam parameters [4–7], with bunch length measurement being particularly challenging. This work employs deep learning to directly extract all the bunch parameters from diffraction images, based on physical correlations between diffraction features and electron beam parameters, achieving the first non-invasive bunch length measurement and providing real-time diagnostic tools for UED facilities.

SETUP OF MACHINE PARAMETERS

Based on the MeV UED under construction at Huazhong University of Science and Technology [8–13], the system employs a 1.4-cell photocathode RF gun, driven by 266-nm ultraviolet laser to generate photoelectrons from a copper cathode. The 2856-MHz RF cavity provides an accelerating gradient of 76.6 MV/m, accelerating the electron beam to 3 MeV. The beam transport line features a solenoid lens positioned 0.2-m downstream of the cathode to compensate for space charge effects and control the transverse beam size at the sample position. After traversing a 1-m drift distance, the electron beam impinges on a polycrystalline aluminum sample, forming distinct diffraction ring patterns on the detector downstream. To systematically investigate the correlation between bunch parameters and diffraction images, we employed the ASTRA particle tracking simulations [14] with the diffraction utilizing the familiar polycrystalline aluminum sample. The initial bunch charge was set to 1 pC, using 5×10^4 macroparticles to adequately account for space charge effects. By adjusting key parameters including the laser spot size, RF phase, and laser pulse duration, we systematically swept the complete parameter space relevant to the experiment, including the transverse horizontal and vertical beam sizes from 0.014 to 1.28 mm, the transverse horizontal and vertical beam divergences from 0.005 to 3.33 mrad, the bunch length ranging from 96.2 to 546 fs, and the energy spread varying from 2.387 to 23 keV.

NUMERICAL METHOD

Diffraction images contain rich bunch parameter information. Transverse beam size broadens diffraction rings through geometric convolution effects; beam divergence causes the final electron momentum to be the vector sum of transverse momentum and diffraction momentum transfer, resulting in image displacement and distortion; energy spread produces radial blurring in higher-order rings through Bragg angle dispersion; bunch length measurement is based on pump-probe principles. A complete diffraction image generation workflow is developed based on kinematic diffraction theory, calculating scattering probability distributions through elastic scattering theory and determining relative intensities of diffraction rings according to structure factors. More specifically, finite bunch length modifies dynamic curves through temporal convolution, causing slower decay edges and reduced oscillation amplitudes in diffraction intensity changes. Detailed analysis of temporal evolution curve characteristics enables bunch length reconstruction and can in principle achieve the non-invasive bunch length measurement based on diffraction images.

Figure 1 illustrates our numerical methodology: impact of electron beam on the sample generates diffraction images, with neural networks extracting bunch parameters. Two spe-

* Email: jcytsai@hust.edu.cn

ISBN: 978-3-95450-279-0 ISSN: 3043-0208 doi: 10.18429/JACoW-SAP2025-FRNC2

THE START-TO-END BEAM DYNAMICS SIMULATION STUDY AND ITS APPLICATION IN THE HIGH-INTENSITY CYCLOTRON OF CIAE*

Tianjian Bian†, Fengping Guan, Shizhong An, Sumin Wei, Luyu Ji, Jinrong Lu, Lin Dai, Ruijin Liu, Yuzhuo Huang, Peng Huang, China Institute of Atomic Energy, Beijing, China

Abstract

The beam dynamics simulation technology for cyclotrons is relatively mature, however, it is typically implemented independently in each subsystem and assumed initial conditions are introduced multiple times, making it difficult to obtain quantitative results and carry out a global optimized design. Precise and quantitative start-to-end beam dynamics simulations facilitate a better understanding of the complex beam dynamics behaviours, which is one of the key technologies for high-intensity accelerators. In this paper, start-to-end (S2E) beam-dynamics simulations are performed for an 18 MeV/1 mA high-intensity cyclotron. Every subsystem, the injection line, spiral inflector, central region, acceleration region, extraction region and uniform beam-transport line, is modelled quantitatively. Furthermore, the central region is optimized by S2E method and the resulting gain in beam performance is evaluated.

INTRODUCTION

The neutron yield of the neutron source based on the 18 MeV/1 mA high-intensity cyclotron developed by the China Institute of Atomic Energy (CYCIAE-18) has reached 7×10^{13} n/s and has been successfully applied in high-resolution neutron imaging and Boron Neutron Capture Therapy (BNCT) experiments. In high-intensity cyclotrons, global optimisation of beam dynamics and minimisation of beam loss are essential. Traditionally, cyclotron beam-dynamics simulations are usually performed section-by-section with assumed initial conditions. Although efficient, this approach introduces cumulative errors that prevent quantitative analysis in high-intensity, beam-loss-sensitive machines.

Start-to-end (S2E) simulations provide high-fidelity predictions of accelerator performance and enable global optimisation [1]. The S2E method are used to simulate the beam dynamics of CYCIAE-18, includes injection line, spiral inflector, central region, acceleration and extraction region, uniform beamline, etc. Based on S2E method, the radial-phase space as a metric is proposed to optimise the central region for higher beam quality and the corresponding improvement in beam performance is evaluated. Furthermore, this paper proposes a uniform beamline based on combined-function quadrupole-octupole magnets, and experimental results show 83% uniformity.

* Work supported by Sustained Support Research Project (Grant No. BJ040261224908), the National Natural Science Foundation of China (Grant No. 12375156), China National Nuclear Corporation Fundamental Research Project (Grant No. CNNC-JCYJ-202404) and Nuclear technology research and development (Grant No.HJSYF2025(11)).

† biantianjian@foxmail.com or biantianjian@ciae.ac.cn

INJECTION LINE

The injection beamline focuses and bunches the 35 keV beam from the H^- ion source. The CYCIAE-18 employs two solenoids with a buncher positioned between them. For high-intensity beams, the space-charge effect is significant in the injection line, so solenoid fields of more than 2000 Gs is required to counteract it. The normalized emittance at the ion source is 0.240 π mm·mrad. With increasing the current, nonlinear space-charge forces drive emittance growth at the injection line exit, as shown in Figure 1. At 5 mA, the emittance reaches 0.274 π mm·mrad.

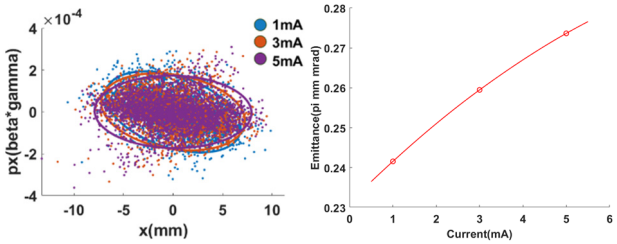

Figure 1: Phase space (left plot) and the emittance growth as function of current (right plot).

Six-dimensional phase space coordinates at the injection-line exit provide the initial conditions for the spiral inflector simulation.

SPIRAL INFLECTOR

The spiral inflector bends the axially injected beam into the median plane. The axial defocusing and longitudinal stretching inside it cause beam loss and quality degradation. Figure 2 illustrates the longitudinal defocusing effect: (a) shows the longitudinal phase space at the inflector inlet and outlet, and (b) the particle-density distribution in phase. The inflector electric field increases the energy spread and flattens the particle-density peak, thereby reducing the beam capture efficiency in central region.

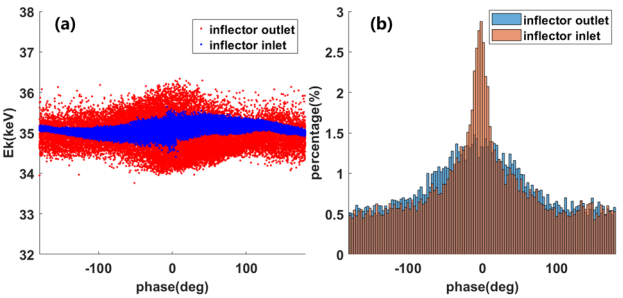

Figure 2: The longitudinal phase space (a) and the particle-density distribution (b).